ACS OMEGA

Open Access

http://pubs.acs.org/journal/acsodf

Article

DFT Investigation of the Stereoselectivity of the Lewis-Acid-Catalyzed Diels−Alder Reaction between 2,5-Dimethylfuran and Acrolein

Mohamed Chellegui, Mahmoud Trabelsi, Benoît Champagne, and Vincent Liégeois*

Cite This: *ACS Omega* 2025, 10, 833−847

Read Online

ACCESS | Metrics & More | Article Recommendations | Supporting Information

ABSTRACT: Density functional theory (DFT) has been enacted to study the Diels−Alder reaction between 2,5-dimethylfuran (2,5-DMF), a direct product of biomass transformation, and acrolein and to analyze its thermodynamics, kinetics, and mechanism when catalyzed by a Lewis acid (LA), in comparison to the uncatalyzed reaction. The uncatalyzed reaction occurs via a typical one-step asynchronous process, corresponding to a normal electron demand (NED) mechanism, where acrolein is an electrophile whereas 2,5-DMF is a nucleophile. The small endo selectivity in solvents of low dielectric constants is replaced by a small exo selectivity in solvents with larger dielectric constants, such as DMSO. In the catalyzed process, the LA interacts with acrolein, forming a O-LA coordinating bond, that enhances its electron-acceptor character, further favoring the NED mechanism and reducing the activation energy. When $AlCl_3$ and $GaCl_3$ catalyze the reaction, the bond formations of both the endo and exo pathways occur via a two-step asynchronous process. Thus, these processes involve the formation of two transition states and a stable intermediate. The second transition state is the critical one and it dictates the increase of the exo selectivity, in comparison to the uncatalyzed reaction. The DFT calculations have also unraveled that the LA plays additional roles, i.e. it forms stable complexes with the carbonyl group of acrolein while $AlCl_3$ and $GaCl_3$ form dimers, which also impact the different equilibria.

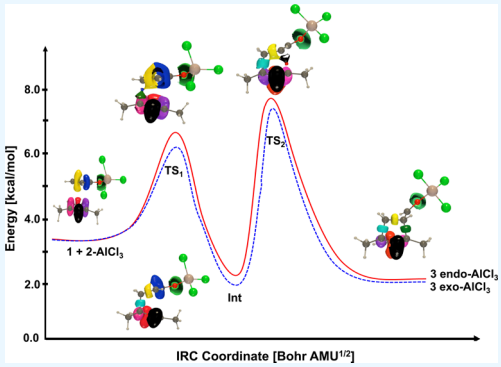

1. INTRODUCTION

Owing to its potential as renewable resource to reduce the dependence on petroleum-based resources biomass has focused considerable attention toward the development of sustainable processes to produce aromatic chemicals, such as benzene, toluene, and xylenes. This refers to the fact that these chemicals are widely used in fuels and in the chemical industry as precursors of polymers.[1−3] In particular, *p*-xylene (PX) is a basic precursor for the synthesis of terephthalic acid,[4−6] which is a monomer to produce polyethylene terephthalate (PET). PET is largely used to fabricate synthetic fibers and plastic bottles owing to its mechanical and chemical properties. Given the rapid and increasing growth of the global PET market (6−8% of PET per year),[7] the synthesis of PET from a renewable raw material has become an area of major interest in an industrial scale and in the field of scientific research.[8] In parallel, the synthesis of liquid fuels and organic chemicals from biomass has recently drawn much interest as an alternative for mitigating the dependence on fossil fuel sources.[9−12] Biomass is one of the most abundant renewable carbon resources in the world for the production of fuels and chemicals.[13,14] Its energy recovery yields 5-hydroxymethylfurfural (5-HMF), a chemical platform at the origin of a wide variety of chemical fuels,[15] that is obtained through the catalytic dehydration of carbohydrates (glucose, fructose, etc.).[16−19] In addition, 5-HMF is a versatile intermediate, and the source of several high added-value chemicals. From this perspective, it has been called a "sleeping giant" in the field of chemical intermediates from biobased raw materials.[20] The catalytic conversion of 5-HMF gives 2,5-dimethylfuran (2,5-DMF) that can be used as a fuel or a transport additive.[21]

Currently, new methods of synthesizing biobased PX from biomass-based raw materials have been elaborated. In this context, several experimental and quantum chemistry studies of the Diels−Alder (DA)[22,23] reactions between 2,5-DMF and multiple alkenes including ethylene,[24−29] maleic anhydride,[30,31] acrylic acid,[32,33] and acrolein,[34] with subsequent dehydration have displayed its very promising potential for the production of renewable PX and other aromatic derivatives with high stereospecificity.

Shiramizu et al.[34] studied the DA reaction between 2,5-DMF and acrolein. The intermediate product obtained after dehydration and decarboxylation provides PX, and subse-

Received: August 27, 2024
Revised: December 9, 2024
Accepted: December 17, 2024
Published: January 1, 2025

quently leads to terephthalic acid. They demonstrated that, (i) this reaction requires a low temperature (T = −60 °C) to proceed effectively, which is an economic limitation for industrial scale applications, (ii) this reaction is thermodynamically controlled for both the endo ($\Delta_r H°$ = −6.41 kcal mol^{-1} and $\Delta_r S°$ = −0.03 kcal mol^{-1} K^{-1}) and exo ($\Delta_r H°$ = −6.39 kcal mol^{-1} and $\Delta_r S°$ = −0.03 kcal mol^{-1} K^{-1}) approaches, so that (iii) the endo stereoisomer is slightly predominant, with an endo/exo ratio equal to 1.2. This reaction is the central focus of this contribution.

The importance of the DA reaction for preparing natural products and bioactive compounds has boosted the development of methods to improve the yields and selectivities of the [4 + 2] cycloaddition reactions.[35] In particular, the observation made in 1960 by Yates and Eaton,[36] that the $AlCl_3$ Lewis acid (LA) strongly accelerates the DA reaction, encouraged researchers to develop LA-catalyzed processes.[37,38] Subsequently, their use has considerably extended the scope of the DA reaction, with better kinetics and with modified endo/exo as well as regio selectivities in comparison to the uncatalyzed process.[39] These effects of the catalysts (Brønsted and Lewis acids) as well as of the nature of the solvent on the selectivity of the DA reaction have been studied experimentally, but also using quantum chemical modeling. So, the frontier molecular orbital (FMO) theory and density functional theory (DFT) have been enacted to explain the reactivity, to unravel the reaction mechanism, and to explain the selectivity of these reactions.[40−52] Within the FMO theory,[53] concepts such as the energy gaps [the difference between the energies of the lowest unoccupied molecular orbital (LUMO) and of the highest occupied molecular orbital (HOMO)] and molecular orbital (MO) interactions are used for explaining the DA reactions. This criterion implies that a DA reaction is accelerated provided the HOMO − LUMO gap is minimized. By attaching electron-withdrawing substituents to the dienophile and/or electron-donating groups to the diene, the HOMO − LUMO gap decreases, and subsequently, the polarity of the transition state (TS) and the reaction rate increase.[54−56] After a comprehensive study of organic reactions, based on the analysis of the conceptual DFT (CDFT) indices, Domingo et al.[57,58] proposed the polar DA mechanism, where the feasibility of the reaction is driven by the nucleophilic character of the diene and the electrophilic character of the dienophile. Larger electrophilic and nucleophilic characters increase the reaction rates through more polar TSs. In the same way, they inferred a good correlation between the activation energies of DA reactions and the polar character of the cycloaddition as measured by the global electron density transfer (GEDT) [using the natural bond order (NBO) method] at the corresponding TSs.[59] Likewise, the activation by a LA or by supplying electron-withdrawing substituents to the more electron-deficient reactant reduces the activation energy, and subsequently enhances the polarity of process.[60]

In 2000, using DFT at the B3LYP/6-31G(d) level, Avalos et al.[43] examined the uncatalyzed and Lewis acid (LA)-catalyzed DA reactions between furan and methyl vinyl ketone. They depicted that the LA increases the asynchronicity of this reaction and decreases the activation energies by promoting the formation of the endo stereoisomer. Next, Fraile et al.[44] studied the LA-catalyzed DA reactions between 2,5-DMF/furan with acrylonitrile and methyl acrylate at the B3LYP/6-31G(d)//HF/3-21G(d) levels. They inferred that (i) the cycloadditions of methyl acrylate with 2,5-DMF and furan promote the endo cycloadduct, (ii) the DA reaction between 2,5-DMF and acrylonitrile promotes the exo cycloadduct, and (iii) $AlCl_3$ catalyzes better these cycloadditions than $ZnCl_2$. In the same way, using DFT at the B3LYP/6-31G(d) level, Sáez et al.[46] explored the mechanism of the $AlCl_3$-catalyzed DA reactions between 2-(trimethylsilyloxy)acrolein and furan. They found that (i) this reaction occurs through a three-step mechanism passing through a zwitterionic intermediate, (ii) the endo cycloadduct is the major product, (iii) taking into account the solvent (dichloromethane) effects leads to a better stabilization of the TS and of the intermediate, and (iv) the coordination of $AlCl_3$ with 2-(trimethylsilyloxy)acrolein increases the electrophilicity of the dienophile, and subsequently rises the polarity of this cycloaddition. Using DFT at the B3LYP/6-31G(d) level, Alves et al.[47] 2006 performed a study on the uncatalyzed and LA-catalyzed DA cycloadditions of cyclopentadiene with crotonaldehyde and methacrolein. They asserted that (i) these reactions proceed via a one-step highly asynchronous mechanism, (ii) the reaction of cyclopentadiene promotes the formation of the endo cycloadduct with crotonaldehyde, and the exo product with methacrolein, (iii) the inclusion of catalysts decreases the activation barrier, and (iv) the solvent (PCM/dichloromethane) effects increase the stability of the TSs owing to their zwitterionic character, but do not change the stereoselectivity observed in vacuo.

Later, using DFT/B3LYP/6-31+G(d,p) calculations, Nacereddine et al.[48] tackled the DA reaction between difluoro-2-methylcyclopropane and furan. They emphasized that the endo cycloadduct is favored both kinetically and thermodynamically in comparison to the exo cycloadduct, and that this reaction occurs by a one-step asynchronous mechanism. Besides, employing the B3LYP/6-31G(d) method to describe the uncatalyzed and LA-catalyzed DA reactions of methyl acrylate and methyl methacrylate with furan Bouacha et al.[49] highlighted that (i) these reactions take place via a one-step asynchronous mechanism, (ii) the endo product is both kinetically and thermodynamically favored, and (iii) the inclusion of solvent (PCM/dichloromethane) and catalyst ($AlCl_3$) effects decrease the activation energies but do not modify the stereoselectivity observed in the uncatalyzed DA reactions in vacuo.

Likewise, using DFT at the M06-2X-D3/6-311+G(d,p) computational level, Ju et al.[32] handled the conversion of 2,5-DMF and acrylic acid to aromatic derivatives catalyzed by Brønsted acid ionic liquids in the experimental conditions. They investigated two mechanisms of 2,5-DMF activation: UPOD (unprotonated oxygen of 2,5-DMF) and POD (direct protonated oxygen of 2,5-DMF), each with endo and exo DA reaction routes. They observed that (i) the UPOD route produces a mixture of aromatic products [PX + DMBA (2,5-dimethylbenzoic acid)], with the overall rate limited by the ring-opening step, while (ii) the POD route only yields DMBA, with the DA cycloaddition being the rate-determining step and the energy barrier of the cycloaddition higher than that of UPOD, and (iii) the endo stereoisomer is more favorable than the exo one.

Insights into the Diels−Alder reaction and its stereoselectivity have been unraveled by adopting the distortion/interaction−activation strain (DIAS) scheme,[61,62] which investigates the effects of the reorganization/distortion and interaction energies along the reaction pathway. These studies highlighted the key role of the distortion or strain energy on the relative endo and exo TS energies, and therefore on the

https://doi.org/10.1021/acsomega.4c07888
ACS Omega 2025, 10, 833−847

Scheme 1. Schematic Representation of the Uncatalyzed and LA-Catalyzed DA Reactions between 2,5-DMF 1 and Acrolein 2, [Lewis Acid (LA), endo Cycloadduct (3 endo), and exo Cycloadduct (3 exo)]. [The Experimental Optimized Conditions Reported in ref 33 Are Catalyst = $Sc(OTf)_3$, Solvent = $CDCl_3$, Temperature = −60 °C, Reaction Time = 68.5 h, Yield of the Final Product (endo + exo) = 84%, and $r_{endo/exo}$ = 1.2]

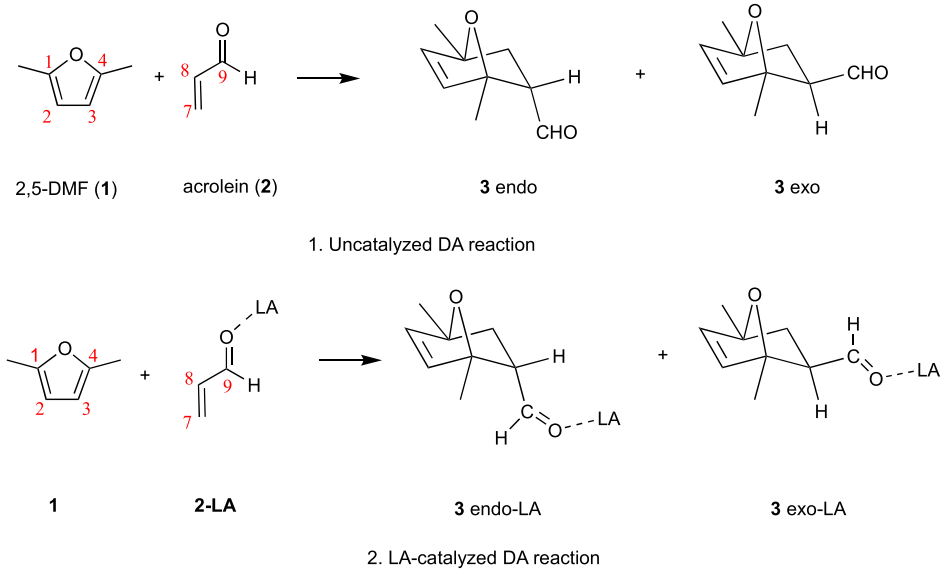

stereoselectivity. Then, when combined with the energy decomposition analysis (EDA) method, this approach allows assessing the relative importance of the electrostatic, Pauli, and orbital interactions contributions. So, Vermeeren et al.[62] have shown that LAs facilitate the DA reaction by reducing the Pauli repulsion between the π-systems of the diene and dienophile.

In this study, DFT is employed to describe the uncatalyzed (Scheme 1.1) and LA-catalyzed DA reactions (Scheme 1.2) between 2,5-DMF **1** and acrolein **2**. These reactions are analyzed both in vacuo and in solution (solvent = cyclohexane, dichloromethane, ethanol, and DMSO) by considering typical catalysts of group 13, $AlCl_3$, BF_3, and $GaCl_3$. This study also includes the DFT simulation of the $Sc(OTf)_3$-catalyzed DA reaction between 2,5-DMF and acrolein in chloroform in order to assess the obtained results with those found experimentally.[34] In each case, the structural, electronic, and thermochemical properties of the reactants, transition states, and products are evaluated and analyzed. The work is structured as follows: the next Section describes the key aspects of the computational procedure, the following Section presents and discusses the results, while conclusions are provided in the final Section.

2. THEORETICAL AND COMPUTATIONAL ASPECTS

The equilibrium structures of the reactants, products, and transition states were optimized at the DFT level using the M06-2X exchange−correlation (XC) functional[63] and the 6-311+G(d,p) basis set. Vibrational frequencies were calculated to confirm the stationary character of the reactants, products (no imaginary frequency), and TSs (one imaginary frequency). Departing from each TS, calculations were performed to describe the structures and energies along the intrinsic reaction coordinate (IRC).[64] For all species, reactants, products, and TSs, the energy ($\Delta_r E$, $\Delta E^{\ddagger}$), enthalpy ($\Delta_r H^{\circ}$, $\Delta H^{\ddagger}$), entropy ($\Delta_r S^{\circ}$, $\Delta S^{\ddagger}$), and Gibbs free energy ($\Delta_r G^{\circ}$, $\Delta G^{\ddagger}$) of both reaction and activation were evaluated. Solvent effects were included in both geometry optimizations and the subsequent calculations of the thermodynamical state functions by adopting the integral equation formalism (IEF) version of the polarizable continuum model (IEF-PCM).[65] This scheme models the solvent by a continuum and its dielectric permittivity (ε). Several solvents have been considered, cyclohexane (ε = 2.02), dichloromethane (ε = 8.93), ethanol (ε = 24.5), and DMSO (ε = 46.7). Calculations were initially performed for T = 298.15 K and P = 1.0 atm. Then, a concentration correction of +1.89 kcal mol^{-1} in the calculation of the solvation free energies of cycloaddition was used to account for the change of conditions when going from gas phase at 1 atm to solution at 1 M concentration.[66] This correction was also applied on the in vacuo values in order to better highlight the effects of the surrounding medium. This correction corresponds to a modification of the entropies by −6.34 cal mol^{-1} K^{-1}. In the same way, the reaction rate constants k were calculated based on the Eyring equation,[67] providing the endo/exo ratio ($r_{endo/exo}$), which refers to the difference between the free energies of activation of the endo and exo pathways.

Selecting the $AlCl_3$-catalyzed reaction, Table S1 shows that the M06-2X exchange−correlation functional is a suitable choice, in comparison to higher-level CCSD calculations as well as results obtained with other XC functionals. In particular, the decrease of the activation energy due to the $AlCl_3$ catalysis is closely reproduced as well as the difference of activation energy between the exo and endo pathways of the $AlCl_3$-catalyzed reaction. These M06-2X results are like those obtained with ωB97X-D but quite different from the B3LYP results. These results are consistent with those of our previous study.[29] Yet, the absolute values of the activation energies are slightly underestimated by the M06-2X XC functional with respect to CCSD.

The global electron density transfer (GEDT)[58] at the TSs was computed as the sum of the natural atomic charges (q), obtained by a natural bond orbital (NBO) analysis,[68] of the atoms belonging to each framework (f) at the TSs; i.e.

https://doi.org/10.1021/acsomega.4c07888
ACS Omega 2025, 10, 833−847

Table 1. Electronic Properties (eV), ε_H, ε_L, $\mu = (\varepsilon_H + \varepsilon_L)/2$; $\eta = \varepsilon_L - \varepsilon_H$, $\omega = \mu^2/2\eta$, $N = \varepsilon_H$ (Nu) $- \varepsilon_H$ (TCE) [ε_H (TCE) = −10.9 eV (in vacuo)], $\Delta\omega = \omega_{diene} - \omega_{dienophile}$, ΔE(NED) = [ε_L (2) $- \varepsilon_H$ (1)], ΔE(IED) = [ε_L (1) $- \varepsilon_H$ (2)], in vacuo at the M06-2X/6-311+G(d,p) Level

	ε_H	ε_L	μ	η	ω	N	$\Delta\omega$	ΔE(NED)	ΔE(IED)
1	−7.1	0.4	−3.4	7.5	0.8	3.8			
2	−9.3	−1.0	−5.1	8.3	1.6	1.6	−0.8	6.1	9.7
2-AlCl$_3$	−9.7	−3.0	−6.3	6.6	3.0	1.2	−2.2	4.1	10.1
2-BF$_3$	−11.1	−2.6	−6.8	8.5	2.7	−0.2	−1.9	4.5	11.5
2-GaCl$_3$	−9.9	−2.8	−6.3	7.1	2.8	1.0	−2.0	4.3	10.3

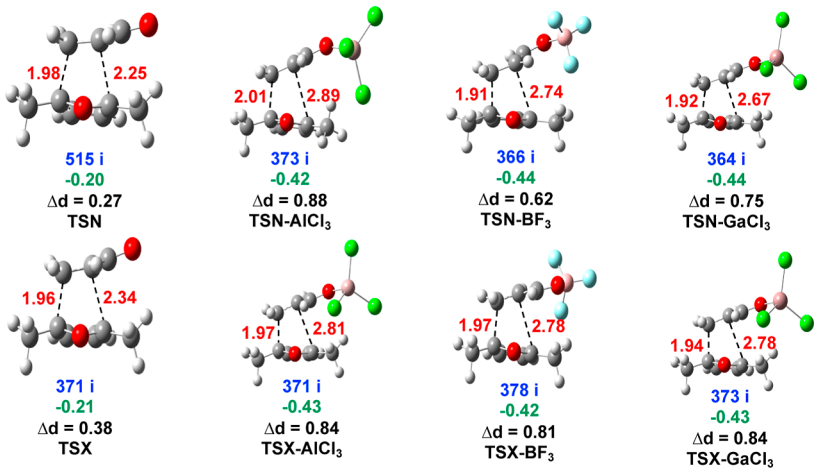

Figure 1. Geometries of the transition states of the uncatalyzed and LA-catalyzed DA reactions in vacuo. The C_1-C_7 and C_4-C_8 distances and the $\Delta d = d_{C_4-C_8} - d_{C_1-C_7}$ values are given in Å. The unique imaginary frequencies, in cm^{-1}, are provided in blue. The GEDT values at the TS, estimated as the charge on the acrolein, in e, are given in green. [*N* = endo, *X* = exo].

GEDT $= \sum_{i\in f} q_i$ Positive values mean an electronic flux from the considered framework to the other one.

A topological analysis within the bond evolution theory (BET)[69] was carried out at the same M06-2X/6-311+G(d,p) level. First, the wave function was obtained for each point of the IRCs and, then, the electronic localization functions (ELF)[70,71] analysis was enacted by using the TopMod package[72] considering a grid step of 0.2 bohr. The ELF basin positions were visualized using DrawMol[73] and the basin populations evolution along the IRC by DrawProfile.[74]

Following the approach of conceptual DFT,[75−77] several descriptors of the electronic structure and reactivity were also evaluated, including the energies of both the HOMO (ε_H) and the LUMO (ε_L), the LUMO − HOMO gap (gap $= \varepsilon_L - \varepsilon_H$), the global electrophilicity ($\omega = \mu^2/2\eta$),[78] the chemical potential [$\mu = (\varepsilon_H + \varepsilon_L)/2$],[75] and the global hardness ($\eta = \varepsilon_L - \varepsilon_H$).[79] The nucleophilicity index (N) was calculated as $N = \varepsilon_H$ (Nu) $- \varepsilon_H$ (TCE) where Nu is the nucleophile and TCE is the tetracyano-ethylene.[80] In addition, the difference between the global electrophilicity indices of the reactants ($\Delta\omega = \omega_{diene} - \omega_{dienophile}$) was evaluated since it determines the polar character of the process.[81]

The thermodynamics and kinetics of the reactions were further examined using the DIAS approach[82−84] to investigate the effects of the reorganization/distortion and interaction energies along the reaction pathway. The distortion energies (ΔE_{Dis}) were calculated by extracting the geometry of a given moiety (i.e., acrolein, 2,5-DMF, and acrolein-$AlCl_3$) in the TS, product, or at any point along the IRC, and performing a single-point calculation to evaluate its total electronic energy and finally subtracting it from its equilibrium-geometry value. Interaction energies (ΔE_{Int}) were then obtained by subtracting the distortion energies from the total electronic energies (relative to the sum of equilibrium-geometry energies of the reactants)

$$\Delta E_{Int} = \Delta E - \Delta E_{Dis}$$

The autoDIAS tool, developed by Svatunek and Houk, was employed to perform the DIAS analysis along the reaction pathways.[85]

All calculations were carried out with the Gaussian16 software package.[86]

3. RESULTS AND DISCUSSION

3.1. Reaction in Vacuo. *3.1.1. Analysis of the CDFT Reactivity Indices of the Reactants.* First, to revealed the role of the 2,5-DMF (**1**), acrolein (**2**), and acrolein−LA (**2-LA**) complexes in these DA reactions, an analysis of the CDFT indices of the reactants, computed at the M06-2X level, was performed (Table 1). In this Section on the reaction in vacuo, only the s-trans conformer of acrolein was considered while a comparative discussion on the reactivity of the s-cis and s-trans conformers is given in Subsection 3.2.

The electronic chemical potential μ of **1** (−3.4 eV) is higher than those of **2** (−5.1 eV), and of the **2-LA** complexes, −6.3 eV (**2-AlCl$_3$**), −6.8 eV (**2-BF$_3$**), and −6.3 eV (**2-GaCl$_3$**), demonstrating that the GEDT in these DA reactions takes place from **1** toward **2** and the **2-LA** complexes. Consequently, the normal-electron demand (NED) mechanism of the uncatalyzed and LA-catalyzed DA reaction is favored with respect to the inverse-electron demand (IED) mechanism. This is confirmed by the smaller value of ΔE(NED) = [ε_L(**2**)

https://doi.org/10.1021/acsomega.4c07888
ACS Omega 2025, 10, 833−847

Table 2. Thermochemical State Functions ($\Delta_r E$, $\Delta_r H°$, $\Delta_r G°$, $\Delta E^‡$, $\Delta H^‡$, $\Delta G^‡$, $\Delta\Delta G^‡$ in kcal mol^{-1} and $\Delta_r S°$, $\Delta S^‡$ in cal mol^{-1} K^{-1}), and the endo/exo Ratio of the Uncatalyzed DA Reaction between 1 and 2 in vacuo at the M06-2X/6-311+G(d,p) Level. $\Delta\Delta G^‡ = [\Delta G^‡$ (TS-endo) $- \Delta G^‡$ (TS-exo)]

reactions	$\Delta_r E$	$\Delta_r H°$	$\Delta_r S°$	$\Delta_r G°$	$\Delta E^‡$	$\Delta H^‡$	$\Delta S^‡$	$\Delta G^‡$	$\Delta\Delta G^‡$	$r_{endo/exo}$
1 + 2 →3 endo	−11.9	−9.7	−44.2	3.4	13.9	14.4	−42.7	27.1	−0.3	1.6
1 + 2 →3 exo	−12.2	−10.0	−43.7	3.3	14.2	14.7	−42.5	27.4		

$- \varepsilon_H(\mathbf{1}) = 6.1$ eV] with respect to ΔE(IED) = [$\varepsilon_L(\mathbf{1}) - \varepsilon_H(\mathbf{2}) = 9.7$ eV].

The electrophilicity and nucleophilicity indices of acrolein amount both to 1.6 eV, **2** being therefore classified as a strong electrophile and a moderate nucleophile within their respective scales.[87] The strong electrophilic character of acrolein originates from the electron-withdrawing (EW) −CHO group. On the other hand, for **1**, ω = 0.8 eV and N = 3.8 eV so that **1** is characterized as a moderate electrophile and as a strong nucleophile. Therefore, 2,5-DMF participates in DA reactions as a strong nucleophile without the need for a nucleophilic activation. Moreover, the uncatalyzed DA reaction has a polar character, as substantiated by the high value of the difference of electrophilicity indices between the two reactants ($\Delta\omega$ = −0.8 eV).

The coordination of the LA with the O atom of the carbonyl group of acrolein **2** (Scheme 1.2) increases considerably its electrophilicity but decreases its nucleophilic character. The ω index of the **2-LA** complexes is a function of the metal, increasing in the Al > Ga > B order. Moreover, the LA reduces ΔE(NED), which remains smaller than ΔE(IED) (Table 1). Therefore, the LA-catalyzed processes are more polar than uncatalyzed ones.

3.1.2. Thermodynamic and Kinetic Analysis. 3.1.2.1. Uncatalyzed DA Cycloaddition. The uncatalyzed DA reactions can occur through two stereoisomeric reaction channels, namely endo and exo (Scheme 1.1). The structures of the TSs together with the C_1-C_7 and C_4-C_8 bond lengths are portrayed in Figure 1. Table 2 lists the reaction and activation energies, as well as the activation Gibbs free energy differences ($\Delta\Delta G^‡$), and the endo/exo kinetic ratio ($r_{endo/exo}$). The DA reaction between **1** and **2** is exothermic ($\Delta_r H°<0$), but slightly endergonic ($\Delta_r G°>0$). Furthermore, the formation of the exo cycloadduct is slightly more exothermic than that of the endo one. The **3 exo** product is thermodynamically slightly more stable than the **3 endo** product [$\Delta_r X$ (**3 exo**) < $\Delta_r X$ (**3 endo**), with X = E, $H°$, and $G°$] (with differences of the order of the accuracy of the method). On the other hand, the endo stereoisomer is kinetically favored with an endo/exo kinetic ratio of 1.6.

At the TSs, the lengths of bonds under formation (C_1-C_7 and C_4-C_8) are 1.98 and 2.25 Å for the TS-endo (TSN), while 1.96 and 2.34 Å for the TS-exo (TSX) (Figure 1). Their differences, namely Δd = [$d(C_4-C_8) - d(C_1-C_7)$], are used to characterize the asynchronicity on the bond formation, with values of 0.27 and 0.39 Å for the endo and exo mechanisms, respectively. They demonstrate that these uncatalyzed cycloadditions take place via a one-step asynchronous mechanism, with the exo pathway being slightly more asynchronous than the endo one. The nature of the vibrational normal coordinate associated with the unique imaginary frequency of these TSs (Figure 1) indicates that it mainly concerns the motion of the C_1, C_7, C_4, and C_8 atoms along the C_1-C_7 and C_4-C_8 bond formations. The GEDT values at the TSs, −0.20 e and −0.21 e for the endo and exo pathways, respectively, account for the polar character of these DA reactions. The flux of the electron density goes from the 2,5-DMF moiety to the acrolein one, in agreement with the larger chemical potential of **1** (−2.4 eV) than of **2** (−5.1 eV) (Table 1). Thus, these reactions are classified as forward electron density flux (FEDF) reactions.

3.1.2.2. LA-Catalyzed DA Cycloadditions. The activation Gibbs free energies ($\Delta G^‡$), the $\Delta\Delta G^‡$ differences, and the $r_{endo/exo}$ of the LA-catalyzed reaction between **1** and **2** (Scheme 1.2) are summarized in Table 3. The TSs corresponding to the formation of both stereoisomers, endo and exo are illustrated in Figure 1. The LA catalysts decrease the activation barrier by up to 17 kcal mol^{-1}. In addition, the exo stereoisomer is now clearly kinetically favored with $\Delta\Delta G^‡$ values of 1.0, 2.6, and 1.9 kcal mol^{-1} for $AlCl_3$, BF_3, and $GaCl_3$, respectively. BF_3 is the most exo selective LA catalyst. Likewise, for both mechanisms, $AlCl_3$ leads to the largest reduction of the activation barrier (Table 3). This refers to the fact that the complexation of acrolein **2** with $AlCl_3$ is more stabilizing than that with $GaCl_3$ and BF_3 [$\Delta_c X$(**2-AlCl$_3$**) < $\Delta_c X$(**2-GaCl$_3$**) < $\Delta_c X$(**2-BF$_3$**), with X = E, $H°$, and $G°$, Table S10]. Therefore, the corresponding decomplexation is also less feasible [$\Delta_d X$(**3-AlCl$_3$**) > $\Delta_d X$(**3-GaCl$_3$**) > $\Delta_d X$(**3-BF$_3$**), for both endo and exo pathways, Table S12], which refers to the formation of a strong coordinating bond between the O atom of the carbonyl group and $AlCl_3$. In the same context, the DFT calculations show that the complexation reaction of LAs with acrolein is exothermic ($\Delta_c H° < 0$) and exergonic ($\Delta_c G° < 0$) (Table S10). In parallel, all the LAs decomplexation reactions are endothermic [$\Delta_d H°$(**3-LA**) > 0] and endergonic [$\Delta_d G°$(**3-LA**) > 0] for both the endo and exo pathways in vacuo (Table S12).

The Δd values range between (0.75−0.88 Å) and (0.81−0.84 Å) for the endo and exo mechanisms, respectively (Figure 1). Thus, while the mechanism remains one-step the TSs is typical of highly asynchronous bond-formation processes, with TSX-LA more asynchronous than TSN-LA. The vibrational normal coordinate of the imaginary frequency mode keeps the same character in presence of LA. Then, the GEDT values amount to −0.43 e for both endo and exo pathways, highlighting a larger flux of the electron density from 2,5-DMF to the acrolein−LA complex than for the uncatalyzed

Table 3. Activation Gibbs Free Energy ($\Delta G^‡$ in kcal mol^{-1}), Activation Gibbs Free Energy Differences ($\Delta\Delta G^‡$ in kcal/mol), and the endo/exo Kinetic Ratio of the LA-Catalyzed DA Reaction between 1 and 2 In Vacuo at the M06-2X/6-311+G(d,p) Level

reactions	$\Delta G^‡$	$\Delta\Delta G^‡$	$r_{endo/exo}$
1 + 2-AlCl$_3$ →3 *endo*-AlCl$_3$	10.8	1.0	0.2
1 + 2-AlCl$_3$ →3 *exo*-AlCl$_3$	9.8		
1 + 2-BF$_3$ →3 *endo*-BF$_3$	15.6	2.6	0.01
1 + 2-BF$_3$ →3 *exo*-BF$_3$	13.0		
1 + 2-GaCl$_3$ →3 *endo*-GaCl$_3$	13.4	1.9	0.04
1 + 2-GaCl$_3$ →3 *exo*-GaCl$_3$	11.5		

https://doi.org/10.1021/acsomega.4c07888
ACS Omega 2025, 10, 833−847

reaction. This corresponds to a more polar reaction, consistently with a larger $\Delta\omega$ value, a smaller HOMO − LUMO gap, and an increase of the electrophilicity index of the acrolein (Table 1) with respect to that of the uncatalyzed reaction. In summary, the LA increases both the degree of asynchronicity and the polarity of the process but does not change the reaction mechanism.

3.2. Solvents Effects. *3.2.1. Analysis of s-cis and s-trans Isomers of Acrolein.* Acrolein exhibits two distinct geometric isomers, namely s-cis and s-trans. DFT calculations at the IEFPCM(dichloromethane)/M06-2X/6-311+G(d,p) level of approximation demonstrate that the energy, enthalpy, and Gibbs free energy of the s-cis conformer exceed those of the s-trans conformer (Table S3). Consequently, the s-trans conformer exhibits a significantly higher Maxwell−Boltzmann weight (P = 98%) compared to the s-cis one (P = 2%). This is why, for the investigation of the DA reaction between 2,5-DMF **1** and acrolein **2** targets in priority its s-trans conformation, while some discussions are added on the s-cis/s-trans comparison. Then, besides when it is noted, in the following Sections and Subsections, the discussion deals implicitly with the s-trans conformation.

3.2.2. Uncatalyzed DA Cycloaddition. The reaction and activation energies, the $\Delta\Delta G^{\ddagger}$ differences, and the $r_{endo/exo}$ for the uncatalyzed reaction in solution (cyclohexane, dichloromethane, ethanol, and DMSO) are given in Table S4. The structures of the TSs are plotted in Figure S1. $\Delta_r H^\circ$ and $\Delta_r G^\circ$ reveals little or no effect of the solvent, increasing $\Delta_r G^\circ$ by less than 0.8 kcal mol^{-1} with the dielectric constant of the medium for both the endo and exo mechanisms. Likewise, the solvent has a small impact on $\Delta G^{\ddagger}$, with a reduction of the activation barrier from 0.2 to 1.2 kcal mol^{-1} across the range of examples (Figure 2). This contradicts the FMO theory prediction,

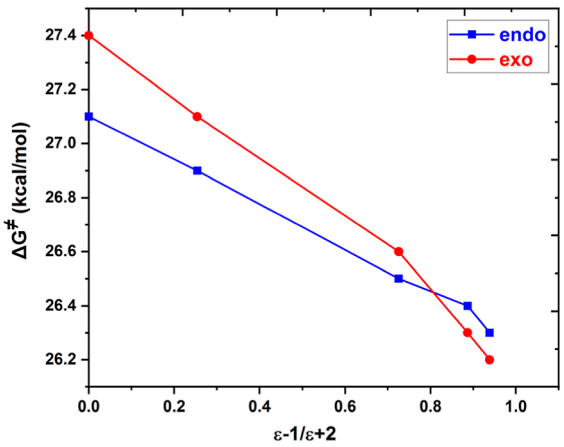

Figure 2. Variation of the Gibbs free energy of activation for the uncatalyzed DA reaction between 2,5-DMF and acrolein plotted as a function of solvent polarity, estimated by the $(\varepsilon - 1)/(\varepsilon + 2)$ function. For comparison the $\Delta G^{\ddagger}$ in vacuo data have been added $(\varepsilon - 1/\varepsilon + 2 = 0)$.

because the NED gap (which is smaller than the IED gap in all cases) increases with the solvent polarity, while the activation energy changes in the opposite way.

Then, when the polarity of the solvent increases, $\Delta\Delta G^{\ddagger}$ increases slightly (from −0.2 to 0.1 kcal mol^{-1}, Table S4), and consequently, accounting for solvents effects with larger dielectric constants changes slightly the stereoselectivity of the uncatalyzed DA reaction with respect to the in vacuo situation.

The differences between the lengths of the forming C−C single bonds in the TSs (Figure S1), lie in the (0.31−0.42 Å) range for the TS-endo, and (0.44−0.56 Å) for the TS-exo. They show that these TSs correspond to a one-step asynchronous process, with the TS-exo mechanism being slightly more asynchronous than the TS-endo one (Figure S1). For both mechanisms, the degree of asynchronicity increases slightly with the polarity of the solvent (Figure S1), in parallel with the increase of the GEDT from 2,5-DMF to acrolein.

For the s-cis isomer, the exo product is also slightly thermodynamically favorable, while the endo stereoisomer holds a kinetic preference, with an endo/exo kinetic ratio of 1.7, in comparison to 1.2 for s-trans (Table S5).

3.2.3. LA-Catalyzed DA Cycloadditions. In solution, the LA-catalyzed DA reaction between 2,5-DMF and acrolein (Scheme 1.2) is characterized by the formation of two TSs (TS_1 and TS_2) and a stable intermediate (Int). Nevertheless, for the endo pathway, only one TS was found when the solvent is polar (different from cyclohexane). The activation energy ($\Delta E^{\ddagger}$), the activation enthalpy ($\Delta H^{\ddagger}$), the activation entropy ($\Delta S^{\ddagger}$), the activation Gibbs free energies ($\Delta G^{\ddagger}$) for the different (endo and exo) TSs, as well as the $\Delta\Delta G^{\ddagger}$ differences, and the $r_{endo/exo}$ are reported in Table S6. The reaction energies associated with the formation of the intermediate are gathered in Table S7. The structures of the TSs (TS_1 and TS_2) corresponding to the formation of both stereoisomers are outlined in Figures S2−S7. When there are two transition states, the LA decreases the activation barriers (TS1 and TS2) for both the endo and exo mechanisms (Figure 3). In most of the cases, the activation barriers are smaller for the exo path. Then, when increasing the solvent polarity, the activation barrier to TS1 decreases while it increases for TS2. Consequently, in cyclohexane, $\Delta G^{\ddagger 1}$ is larger than $\Delta G^{\ddagger 2}$ and the kinetic control is dictated by TS1. On the other hand, in polar solvents, $\Delta G^{\ddagger 2}$ is generally larger than $\Delta G^{\ddagger 1}$, and TS2 dictates the selectivity of the reaction.

Between the two TSs, there is a zwitterionic intermediate. Again, except for cyclohexane solution, this intermediate is slightly more stable than the sum of the **2-LA** + **1** reactants. Moreover, the exo intermediate is also more stable than its endo analog. For the **3** *endo*-BF_3 DA reaction in polar solvents, there is only one TS, and thus no intermediate. This has been assigned to the absence of O−BF_3 coordinating bond in the corresponding TSs (Figure S6). In this case, the activation barrier decreases slightly (6.4 kcal mol^{-1} in dichloromethane, 6.8 kcal mol^{-1} in ethanol, and 6.9 kcal mol^{-1} in DMSO) in comparison to the uncatalyzed reaction.

The normal FMOs gaps $[\Delta E(\text{NED}) = \varepsilon_L(\textbf{2-LA}) - \varepsilon_H(\textbf{1})]$ increase slightly, by about tenths of eV, with the dielectric constant (Table S2). This is associated with an increase of $\Delta G^{\ddagger 2}$ and subsequently of the $\Delta\Delta G^{\ddagger 2}$ values (Table S6), showing that solvent effects improve the exo selectivity of LA-catalyzed DA reactions. Finally, the exo stereoselectivity is larger with $AlCl_3$ than $GaCl_3$, and both are smaller than with BF_3, for the reasons explained above.

For the reaction catalyzed by $AlCl_3$, when comparing the activation energies for the s-cis versus s-trans isomers, the same exo stereoselectivity is observed while the barrier of activation remains smaller for the first TS than the second one. So, the conformation of acrolein does not modify the stereoselectivity of the LA-catalyzed DA reaction (Table S8). In the same way,

https://doi.org/10.1021/acsomega.4c07888
ACS Omega 2025, 10, 833−847

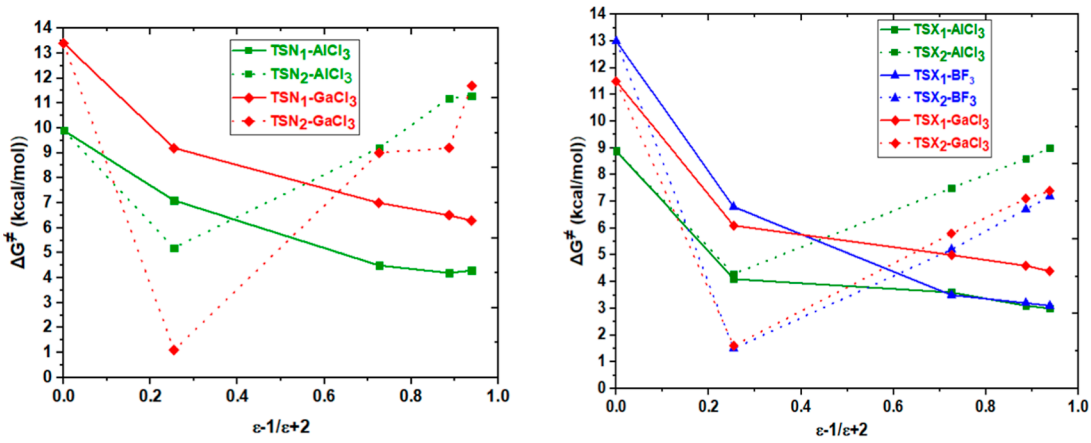

Figure 3. Variation of the Gibbs free energy of activation for the LA-catalyzed DA reaction between 2,5-DMF and acrolein plotted as a function of solvent polarity, represented by the $(\varepsilon - 1)/(\varepsilon + 2)$ function. For comparison the $\Delta G^{\ddagger}$ in vacuo data have been added $(\varepsilon - 1/\varepsilon + 2 = 0)$, though the reactions correspond to a one-step process.

when starting from the s-trans conformer the formation of zwitterionic intermediate (Int) is thermodynamically slightly more stable than its formation when starting from the s-cis one [$\Delta_{int}X$ (s-trans) < $\Delta_{int}X$ (s-cis), with $X = E$, $H°$, and $G°$, Table S9].

The molecular structures at the TS show an increase of asynchronicity of the LA-catalyzed DA reactions in solution in comparison to the uncatalyzed ones, for the first TS (Figures S2−S5). Yet, the degree of asynchronicity decreases slightly with the solvent polarity, in contrast to the uncatalyzed reaction. Their polarity is also larger, with small differences between the two TSs and a minor impact of the solvent polarity. This is consistent with the variation of the CDFT indices of the reactants with the polarity of the solvent (a slight decrease in the electrophilicity and nucleophilicity indices of **2-LA**, and a slight increase of the NED gaps, Table S2). Differences between the exo and endo paths are small with, often, slightly more polar, and asynchronous characters for the endo one.

3.3. Complexation Reactions Involving the LA Catalysts. The LA is not only impacting the position of the TSs (geometries and energies). It can also react with acrolein, with itself, and with the solvent. This has effects on the global thermodynamics and kinetics. First, it forms a stable complex with **2**, where its O atom complexes the central B, Al, and Ga atom of the LA. The **2-LA** complex is particularly stable with $AlCl_3$, being characterized by $\Delta_c G°$ values ranging from −23 to −27 kcal mol^{-1} as a function of the solvent (Table S10). The complexation of **2** with $GaCl_3$ gives $\Delta_c G°$ values from −16 to −19 kcal mol^{-1}, while they are even smaller with BF_3, from −4 to −10 kcal mol^{-1}. Moreover, a sufficiently polar solvent such as DMSO (ε = 46.7) and ethanol (ε = 24.5) further stabilizes the acrolein−LA complex. The energies of complexation are little impacted by the conformation of the acrolein, with variations of the order of 1 kcal mol^{-1} [Table S11].

For the complex between the product (endo and exo) and $AlCl_3$, where the interaction occurs with the O atom of carbonyl group, it is again more stable with $AlCl_3$, having dissociation Gibbs free energies ranging from 24 to 27 kcal mol^{-1} as a function of the solvent (Table S12). These $\Delta_d G°$ values are smaller when looking at the liberation of $GaCl_3$, ranging from 17 to 18 kcal mol^{-1}, while, for BF_3, the $\Delta_d G°$ values go from 4 to 5 kcal mol^{-1}, respectively. The energies of dissociation are minimally affected by the conformation of acrolein, with variations typically less than 1 kcal mol^{-1} [Table S13].

Yet, along the reaction path where LA activates acrolein one may wonder whether the most favorable coordination corresponds to the situation described above (coordination of the central atom of LA with the oxygen atom of acrolein) or rather to the situation where it is linked to the C3═C4 double bond of acrolein. Using the same level of approximation, the calculations demonstrate that the latter coordination mode is less favorable by about 24−27 kcal mol^{-1} ($AlCl_3$), 8−16 kcal mol^{-1} (BF_3), and 16−20 kcal mol^{-1} ($GaCl_3$) (Table S14).

In addition, for the catalyzed reaction, another mechanism can involve the complexation of the C1 and C4 atoms of the 2,5-DMF by the LA, which leads to the inverse electron-demand (IED) LA-catalyzed DA reaction. Keeping the same level of approximation, the calculations indicate that the latter coordination mode is less favorable by about 9−13 kcal mol^{-1} ($AlCl_3$), 4−5 kcal mol^{-1} (BF_3), and 16−20 kcal mol^{-1} ($GaCl_3$) (Table S15) than that involving the complexation between LA and the O atom of carbonyl group of acrolein. For the IED LA-catalyzed DA reaction, another mode of coordination of LA can occur. It corresponds to the case where the O atom of the furan complexes the LA. Calculations lead also to the conclusion that the latter coordination mode is even less favorable than the coordination of LA with the C1 and C4 atoms of the 2,5-DM, by about 3−4 kcal mol^{-1} ($AlCl_3$), 1 kcal mol^{-1} (BF_3), and 7−9 kcal mol^{-1} ($GaCl_3$) (Table S15). In summary, the coordination of the central atom of LA with the O atom of acrolein is the most favored complexation mode.

Another aspect to consider in these LA-catalyzed reactions is the well-known dimerization of $AlCl_3$ and $GaCl_3$. The thermodynamic dimerization data are provided in Table S16 for the reactions in vacuo and in solution. These dimerization reactions have exothermic and exergonic characters, so that the formation of the Al_2Cl_6 and Ga_2Cl_6 dimers is favored. The $AlCl_3$ dimerization is more exothermic and exergonic than the $GaCl_3$ one. This is related to the similar size of the Al and Cl atom and not to the electronegativity, since Ga is more electronegative than Al. As a matter of fact, the thermodynamics of the **2-LA** complex formation should account for the fact that dimers are the starting structures of these LA and they should be dissociated before forming a complex with **2**.

https://doi.org/10.1021/acsomega.4c07888
ACS Omega 2025, 10, 833−847

Thus, the complexation energies become $\Delta_{c(d)}G^\circ = \Delta_c G^\circ - \frac{1}{2}\Delta_{dim}G^\circ$ (Table S10). In this context, the 2-$AlCl_3$ complex has a $\Delta_{c(d)}G^\circ$ value ranging, as a function of the medium, from −11.5 to −18.4 kcal mol^{-1}, when considering its formation from the Al_2Cl_6 dimer (Table S10). For the reaction between the Ga_2Cl_6 dimer and acrolein, $\Delta_{c(d)}G^\circ$ values go from −8.2 to −12.6 kcal mol^{-1} (Table S10), as a function of the solvent. In the same way, the dissociation Gibbs free energies of the product−LA complex should account for the subsequent formation of dimers, and they are given by $\Delta_{d(d)}G^\circ = \Delta_d G^\circ + \frac{1}{2}\Delta_{dim}G^\circ$ (Table S12). In the latter situation, the resulting $\Delta_{d(d)}G^\circ$ values range, as a function of the nature of the solvent, from 12.9 to 18.8 kcal mol^{-1} and from 9.2 to 12.4 kcal mol^{-1} for $AlCl_3$ and $GaCl_3$, respectively.

Finally, it is noteworthy that the solvent molecules can complex the LA, and particularly if the latter can play the role of Lewis base. The corresponding thermodynamic values of these LA complexation reactions are listed in Table S17. All the LAs complexation reactions are exothermic ($\Delta_c H^\circ$<0). Then, with cyclohexane and ethanol, all LAs complexation reactions are endergonic ($\Delta_c G^\circ$>0). In the case of $AlCl_3$ and $GaCl_3$ interacting with dichloromethane, the formation of solvent−LA complexes is only slightly exergonic or endergonic so that CH_2Cl_2 cannot displace the LA from its dimer. The situation is different with DMSO where the complexes are more stable than the dimers.

3.4. Global Reaction Diagrams. Considering all reactions or interactions between the reactants and the LA, the relative Gibbs free energy diagram of the uncatalyzed and $AlCl_3$-catalyzed DA reactions between 2,5-DMF **1** and the s-trans acrolein **2** in dichloromethane is drawn in Figure 4. In absence

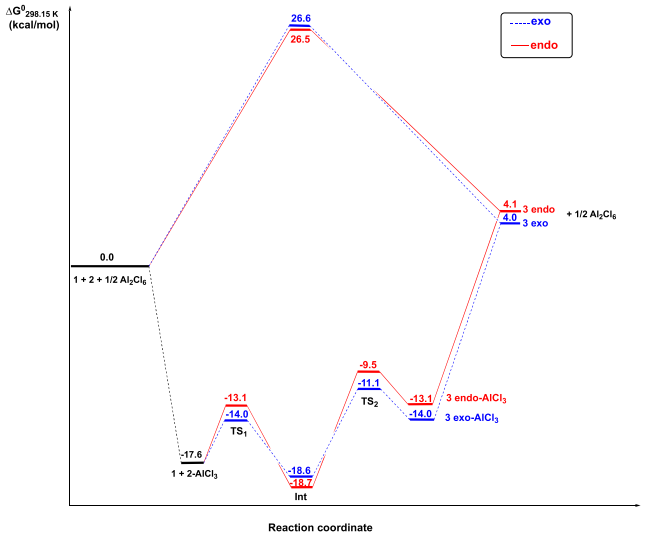

Figure 4. Relative Gibbs free energy diagram (298.15 K) of the uncatalyzed and $AlCl_3$-catalyzed DA reactions between **1** and **2** s-trans at the IEFPCM (dichloromethane)/M06-2X/6-311G+(d,p) level.

of LA, the TS Gibbs free energy relative to those of the isolated reactants ($\Delta G^{\ddagger}$) amounts to 26.5 and 26.6 kcal mol^{-1} for the endo and exo approaches, respectively. When $AlCl_3$ catalyzes the DA reaction, the acrolein−$AlCl_3$ complex is first formed, with a stabilization of 17.6 kcal mol^{-1}. Then, the reaction proceeds via two TSs and one intermediate. The required activation energy to the first TS is smaller than for the second TS. Both activation energies are smaller for the exo pathway (3.6 and 7.5 kcal mol^{-1}) than the endo one (4.5 and 9.2 kcal mol^{-1}). Finally, the product−LA complex is dissociated, which requires 18.0 (exo) or 17.2 (endo) kcal mol^{-1}. This high dissociation free energy suggests that the reaction may terminate at this stage, potentially limiting the product yield. Furthermore, the relative free energy of the final product (∼4.0 kcal/mol) indicates that the global reaction is endergonic. Nevertheless, adding a Lewis base could shift the equilibrium, as seen in Ziegler−Natta polymerizations with organo-aluminum cocatalysts. The global ΔG° reaction diagram obtained with the s-cis isomer of acrolein **2** is like that with s-trans one (Figure S8), with activation energies to both TS1 and TS2 smaller for the exo pathway (4.2 and 8.0 kcal mol^{-1}) than the endo one (5.1 and 9.8 kcal mol^{-1}).

The global ΔG° reaction diagrams obtained with BF_3 and $GaCl_3$ as LA are presented in Supporting Information (Figures S9 and S10). The results with $GaCl_3$ are like those with $AlCl_3$. The following quantitative differences are observed: (i) the **2-LA** complex is less stabilized, (ii) the differences between the activation energies of the first and second TSs are smaller, though the second ones remain larger (6.9 kcal mol^{-1} for the exo and 9.0 kcal mol^{-1} for the endo), and (iii) the **3-LA** dissociation energies are smaller (11−12 kcal mol^{-1}). Then, as far as the exo pathway is considered, the reaction diagram with BF_3 as LA is also qualitatively like those with $AlCl_3$ and $GaCl_3$. Looking at the amplitude of the Gibbs free energy variations, the BF_3 results are closer to those with $GaCl_3$ than $AlCl_3$. On the other hand, along the endo pathway, there is only one TS. The **2-BF_3** complexation energy amounts to −9.1 kcal mol^{-1}, which is like the dissociation energy of **3-BF_3** (8.4 kcal mol^{-1}) while the activation energy (20.1 kcal mol^{-1}) is substantially larger than within the two-step mechanisms.

When the LA is $Sc(OTf)_3$, the LA-activation of the carbonyl group of acrolein **2** stabilizes also the energy of its frontier orbitals, increases its acceptor character (in chloroform, ω = 2.7 eV versus 1.6 eV) and considerably decreases its donor character (in chloroform, N = 0.0 eV versus 1.2 eV). Therefore, the $Sc(OTf)_3$-catalyzed processes is more polar than uncatalyzed ones ($\Delta\omega$ = −1.9 eV versus 0.8 eV, Table S2), and slightly more polar than those catalyzed by $AlCl_3$ and $GaCl_3$, but it is similar to the BF_3-catalyzed one. The complexation reaction of $Sc(OTf)_3$ with acrolein is weaker than that with $AlCl_3$ [$\Delta_c X$(acrolein−$AlCl_3$) < $\Delta_c X$(acrolein−$Sc(OTf)_3$), with X = E, H°, and G°, Table S10]. Calculations did not manage to find the occurrence of a [4 + 2] $Sc(OTf)_3$-catalyzed DA reaction between 2,5-DMF and acrolein. This is be attributed to the significant steric hindrance imposed by the trifluoromethanesulfonate groups and to the presence of a competing [4 + 3] DA reaction. This explanation is similar to what has been mentioned in the context of the DA reaction between cyclopentadiene and 2-silyloxyacroleins.[88] Experimentally, the $Sc(OTf)_3$-catalyzed DA reaction between 2,5-DMF and acrolein exhibited a low yield of *p*-xylene, at low temperatures.

3.5. Distortion/Interaction−Activation Strain (DIAS) Analysis. Following previous investigations on DA reactions and others,[89−91] the DIAS scheme was enacted to further compare the uncatalyzed and catalyzed reactions as well as to compare the exo and endo paths (Figure 5). The uncatalyzed reaction displays a distortion energy that amounts to about twice the corresponding value of the $AlCl_3$-catalyzed reaction. For the uncatalyzed reaction ΔE_{Dis} is mostly attributed to the

https://doi.org/10.1021/acsomega.4c07888
ACS Omega 2025, 10, 833−847

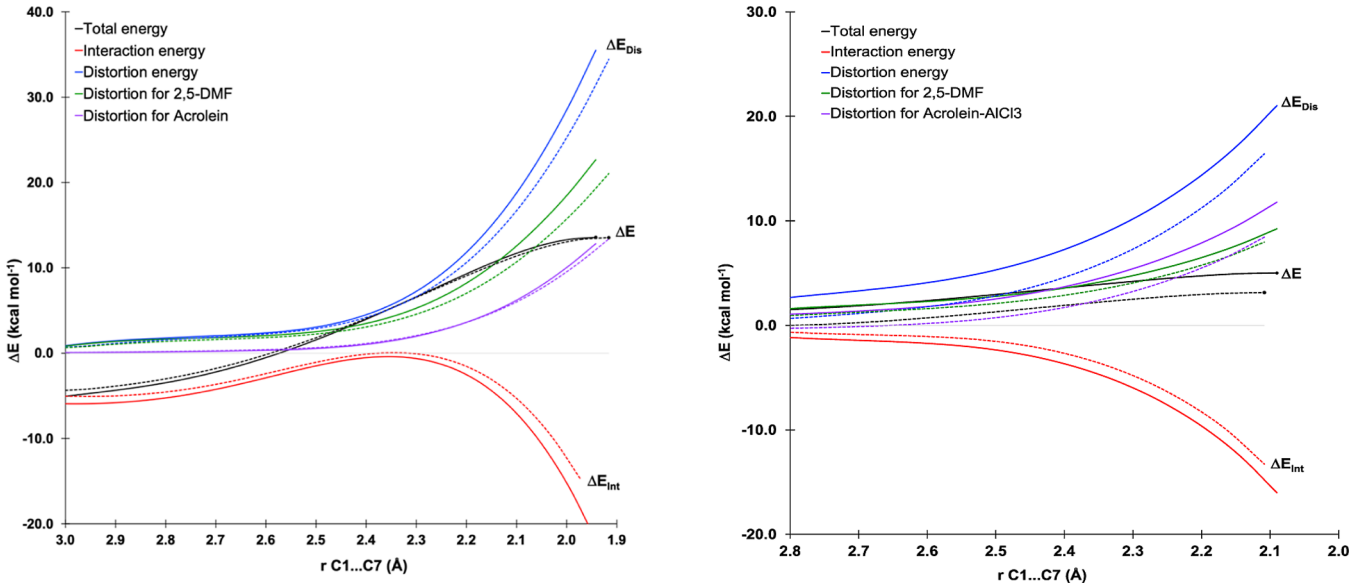

Figure 5. Comparative DIAS diagrams for the endo (solid lines) and exo (dashed lines) approaches of the uncatalyzed (left) and $AlCl_3$-catalyzed (right) DA reactions between 2,5-DMF **1** and acrolein **2** along the reaction coordinate projected onto the forming C···C bond distance as determined with the IEFPCM(dichloromethane)/M06-2X/6-311+G(d,p) method. The transition states are indicated by a dot.

diene whereas for the catalyzed one, ΔE_{Dis} presents similar amplitudes for the diene and the activated dienophile. Figure 5 further shows that the exo selectivity of the catalyzed reaction is attributed to smaller distortion energies, mostly of the $AlCl_3$-activated acrolein, along the IRC path, though the interaction energy is in favor of the endo pathway. The larger ΔE_{Dis} value for the endo pathway is attributed to the closer proximity between the carbonyl-$AlCl_3$ and 2,5-DMF methyl group, $d(Al{-}O{\cdots}CH_3)$ = 3.26 and 3.28 Å, for the endo and exo pathways, respectively.

3.6. Bond Evolution Theory (BET) Analysis along the Decomposition Pathways. To understand the mechanism of the uncatalyzed and $AlCl_3$-catalyzed DA reaction between 2,5-DMF and acrolein, BET analyses were performed for both the endo and exo pathways in dichloromethane. For each BET analysis, the reported basins are those with an increasing or decreasing electron population of along the IRC.

3.6.1. BET Analysis of the Uncatalyzed DA Cycloaddition. The BET study of the TS-endo stereoisomeric pathway of the uncatalyzed DA reaction between 2,5-DMF and acrolein indicates that the process takes place along six SSDs (Figure 6). The BET study of the corresponding TS-exo pathway is similar to that of the endo approach, with only small differences in the population of the basins (Figures S11 and S12). In the **SSD-I**, the system exhibits the topologies of the reactants. Seven basins are highlighted: the V(C2,C3) (2.45 e), V(C1,C2) (3.5 e), and V(C3,C4) (3.5 e) disynaptic basins and the V(O1) (4.2 e, lone pairs) monosynaptic basin of 2,5-DMF as well as the V(C7,C8) (3.2 e) and V(C8,C9) (2.3 e) disynaptic basins and the O2 (5.3 e, lone pairs) monosynaptic basin of acrolein. At the **SSD-II**, two monosynaptic basins are created, V(C1) and V(C7), with 0.5 and 0.3 e. They stem from the concurrent reduction of the V(C1,C2) and V(C7,C8) disynaptic basin populations (Figure 7). These two basins merge in domain **III** to form the new disynaptic V(C1,C7) basin. This corresponds to the formation of the C1−C7 single bond by means of a cusp-C type catastrophe. In the following domains (**SSD-IV** and **SSD-V**), two other monosynaptic

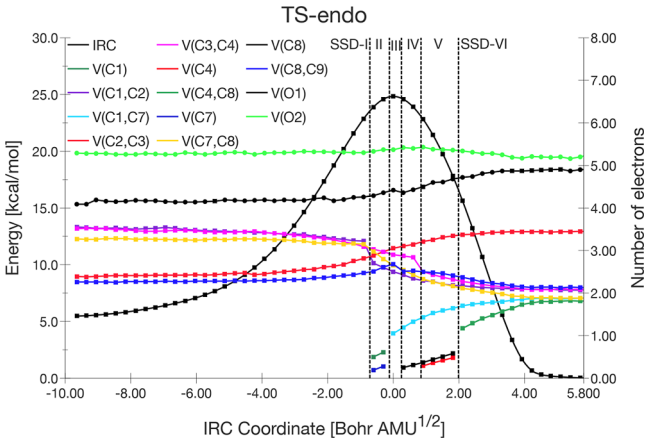

Figure 6. Electron populations (e) evolution for selected basins along the IRC for the endo path of the uncatalyzed DA reaction between 2,5-DMF and acrolein as calculated at the IEFPCM-(dichloromethane)/M06-2X/6-311+G(d,p) level of approximation. These evolutions are depicted on top of the potential energy surface.

basins appear, V(C8) and V(C4) with 0.3 and 0.2 e. They are associated with the simultaneous drop of the V(C4,C3) and V(C7,C8) disynaptic basin populations, respectively by means of 2-fold-F type catastrophes (Figure 7). These two basins join together in domain **VI** to form the new disynaptic V(C4,C8) basin. This leads the formation of the C4−C8 single bond by the means of another cusp-C type catastrophe, and therefore to the final product. Moreover, it is observed that from **SSD-II** to **V**, the population of the disynaptic V(C1,C2), V(C3,C4), and V(C7,C8) basins continuously decrease, which highlights depopulations from double to single bonds. At the same time, the population of the V(C2,C3) basin increases toward a final population of 3.5 e, which corresponds to the transformation of a single into a double bond. During the reaction, the populations of V(O2) and V(C8,C9) remained mostly constant. On the contrary, the V(O1) monosynaptic basin population increases from 4.1 to 4.9 e. This change can be

https://doi.org/10.1021/acsomega.4c07888
ACS Omega 2025, 10, 833−847

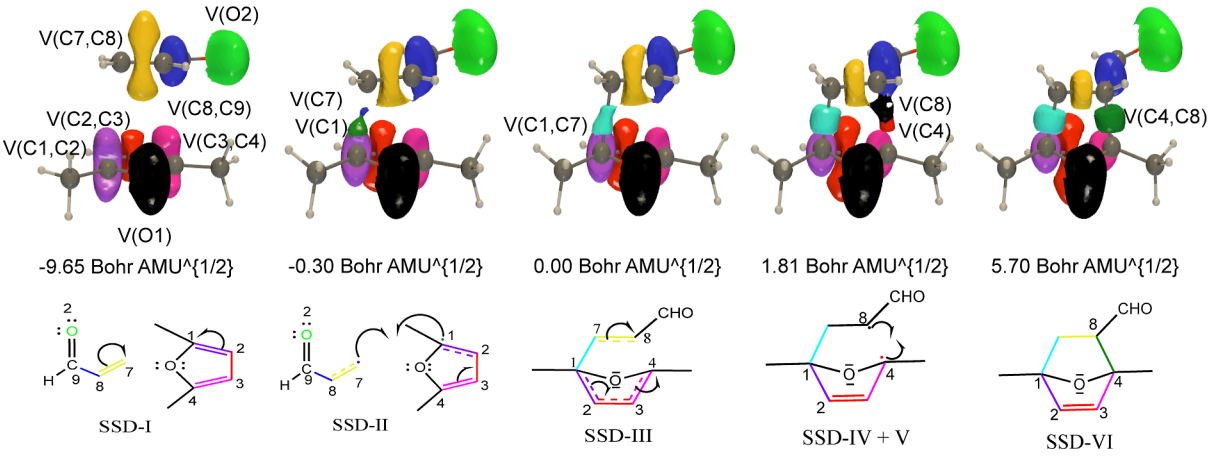

Figure 7. Endo pathway of the uncatalyzed DA reaction between the 2,5-DMF and acrolein: ELF basin isosurfaces for representative points of each of the SSDs found along the IRC and their reaction coordinates. See Figure 6 for the color labeling of the basins. (Half arrows symbolize the transfer of a fraction of electron).

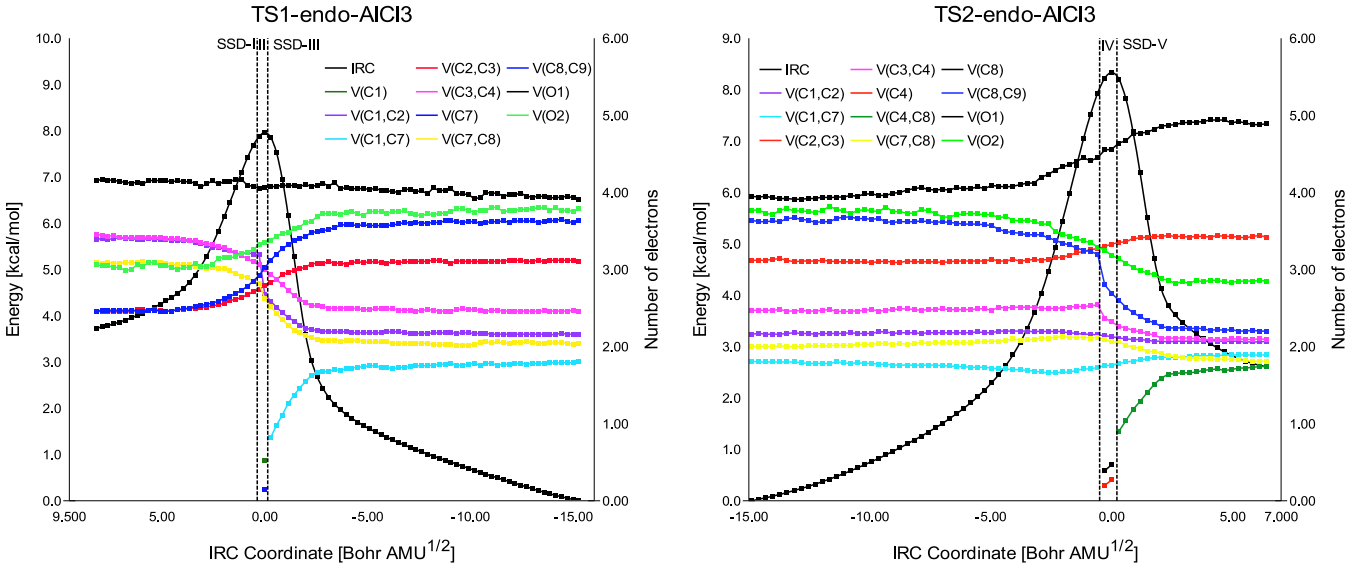

Figure 8. Electron populations (e) evolution for selected basins along the IRC for the endo pathway of the $AlCl_3$-catalyzed DA reaction between 2,5-DMF and acrolein as determined at the IEFPCM(dichloromethane)/M06-2X/6-311+G(d,p) level of approximation. These evolutions are plotted on top of the potential energy surface. The zero energy value (on both reaction steps) corresponds to the intermediate.

explained by the fact that one of the lone pairs of O1 was delocalized in the heteroaromatic ring of the reactant, which reduces its population. This is no more possible in the product.

For comparison, the BET of the uncatalyzed DA reaction between 2,5-DMF and ethylene indicates that the process takes place along three SSDs, as can be seen in Figure S13. Though the number of SSDs is smaller than with acrolein, the mechanism and the evolution of the populations along the IRC are similar. Two conclusions can be drawn from this ELF analysis: (i) the ethylene C7−C8 framework of acrolein presents an identical electronic topology to that of the unsubstituted ethylene, indicating that in the ground state the carbonyl group does not polarize the ethylene framework; and (ii) the activation of the ethylene double bond by an electron-withdrawing group such as an aldehyde group (the case of acrolein in this study) changes the reaction mechanism from a one-step synchronous to a one-step asynchronous mechanism. This activation also leads to a significant increase of the reaction polarity [in vacuo, $\Delta\omega$ (2,5-DMF + acrolein) = from −0.8 eV versus $\Delta\omega$ (2,5-DMF + ethylene) = −0.1 eV] and a decrease in the activation barrier [in vacuo, $\Delta G^{\ddagger}$ (2,5-DMF + acrolein) = 27 kcal mol^{-1} versus $\Delta G^{\ddagger}$ (2,5-DMF + ethylene) = 32.9 kcal mol^{-1}].

3.6.2. BET Analysis of the $AlCl_3$-Catalyzed DA Cycloaddition. The BET study of the endo stereoisomeric pathway of the $AlCl_3$-catalyzed DA reaction between 2,5-DMF and acrolein indicates that the process, involving two TSs and one intermediate, takes place along five SSDs (Figure 8). The BET study of the corresponding TS-exo stereoisomeric pathway is similar, with only slight variations in basins populations (Figures S15 and S16).

In the **SSD-I**, the system shows the topologies of the reactants, taken as 2,5-DMF and the complex between $AlCl_3$ and acrolein. Like for the uncatalyzed mechanisms, seven basins are highlighted: the V(C2,C3) (2.51 e), V(C1,C2) (3.3 e), and V(C3,C4) (3.4 e) disynaptic basins and the V(O1) (4.1 e, lone pairs) monosynaptic basin of 2,5-DMF as well as the V(C7,C8) (3.2 e) and V(C8,C9) (2.5 e) disynaptic basins

https://doi.org/10.1021/acsomega.4c07888
ACS Omega 2025, 10, 833−847

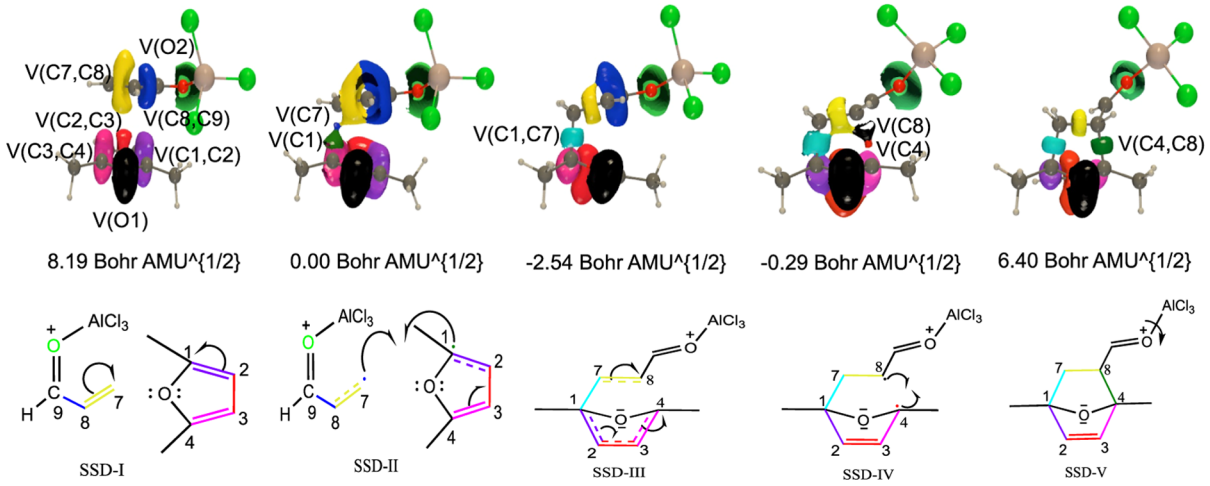

Figure 9. ELF basin isosurfaces for selected points that are representative of each of the SSDs found along the IRC corresponding to the endo transition state of the $AlCl_3$-catalyzed DA reaction between the 2,5-DMF and acrolein and its reaction coordinate. See Figure 8 for the color labeling of the basins. (Half arrow symbolizes the transfer of a fractions of electron).

and the V(O2) (3.1 e, lone pairs) monosynaptic basin of acrolein. This population of the O2 basin is smaller than in acrolein alone, owing to the complexation of $AlCl_3$. At the **SSD-II**, two monosynaptic basins are created, V(C1) and V(C7), with 0.5 and 0.2 e. They result from the simultaneous drop of V(C1,C2) and V(C7,C8) disynaptic basin populations. Similarly to the uncatalyzed reaction, these two basins merge together in domain **III** to form the new disynaptic V(C1,C7) basin, revealing the formation of the C1−C7 single bond by the means of a cusp-C type catastrophe. Moreover, from **SSD-II** to **III**, the population of V(C1,C2), V(C3,C4), and V(C7,C8) basins continuously decreases, which highlights a depopulation from a double to a single bond, while the populations of the V(C2,C3) and V(C8,C9) basins increases with a total population of 3.1 e, which corresponds to the C8−C9 double bond. The population of V(O2) also increases. This situation characterizes the intermediate.

Starting from this intermediate, in the next domain (**SSD-IV**), two other monosynaptic basins appear, V(C4) and V(C8) with similar populations of 0.45 and 0.51 e. They correspond to the simultaneous drop of V(C3,C4) and V(C8,C9) disynaptic basin populations, respectively by means of 2-fold-F type catastrophes (Figure 9). Then, these two basins merge together in domain **V** to form the new disynaptic V(C4,C8) basin, which corresponds to the formation of the C4−C8 single bond by the means of a cusp-C type catastrophe. Similarly, to the uncatalyzed reaction, V(O1) monosynaptic basin population increases from 4.0 to 4.9 e. This change is explained by the fact that one of the lone pairs of the oxygen atom of the reactant was delocalized in the heteroaromatic ring, which reduces its population. On the contrary, the populations of V(O2) and V(C8,C9) basins do not remain constant during the reaction when the catalyst is present. Their populations increase during the first part of the reaction and then decrease in the second part. They appear to play the role of buffer to store the electron density between the two TSs.

4. CONCLUSIONS AND OUTLOOK

The uncatalyzed and Lewis-acid (LA)-catalyzed Diels−Alder reaction between 2,5-DMF and acrolein has been studied by using density functional theory (DFT) with the M06-2X/6-311+G(d,p) level of approximation. These cycloadditions occur along two stereoisomeric reaction channels, namely endo and exo. The uncatalyzed reaction is characterized by a large activation barrier ($\Delta G^{\ddagger} \approx 27$ kcal mol^{-1}, in vacuo) and by a very small endo selectivity ($r_{endo/exo} = 1.6$, in vacuo). This corresponds to a normal electron demand (NED) mechanism where acrolein is an electrophile due the electron-withdrawing carbonyl group whereas 2,5-DMF is a nucleophile. This reaction presents a highly polar character, as evidenced by a large difference of electrophilicity ($\Delta\omega = -0.8$ eV, in vacuo) between the reactants as well as by a high value of the GEDT at the corresponding TS [GEDT ≈ -0.20 e, in vacuo]. The inclusion of solvent effects leads to a slight reduction in the activation barrier, accompanied by a slight increase in the rate constant, and subsequently, a slight decrease in the endo/exo kinetic ratio. In fact, the presence of solvents with larger dielectric constants, such as ethanol and DMSO, makes the reaction exoselective. Moreover, the geometrical structures of the transition state demonstrate that the reaction takes place via a one-step asynchronous process, the TS of the exo path being more asynchronous than that of the endo one.

For the catalyzed reaction, $AlCl_3$, BF_3, and $GaCl_3$ have been selected as LAs. When the LA interacts with acrolein, forming a O−LA coordinating bond, it boosts its acceptor character, further favoring the NED mechanism. This is accompanied by an increase of the polarity of the reaction resulting from the combination between the strong electrophilic character of the acrolein−LA complex and the strong nucleophilic character of 2,5-DMF. As expected, the catalysis is characterized by a reduction in the activation free energy, accompanied by a high decrease in the endo/exo kinetic ratio, so that the LA-catalyzed reaction in polar solvents is exoselective. Using the DIAS scheme enables to demonstrate that (i) the distortion energy associated with $AlCl_3$-catalyzed reaction is about twice smaller than for the uncatalyzed reaction, and that (ii) the exo selectivity of the catalyzed reaction is attributed to a smaller distortion energy (in opposition to more stabilizing interaction energy), mostly of the $AlCl_3$-activated acrolein.

When the reaction is catalyzed in vacuo, the mechanism remains one-step for both endo and exo pathways, and the TSs are representative of highly asynchronous bond-formation processes, with the TS of the exo path being more asynchronous than that of the endo one. On the other hand,

https://doi.org/10.1021/acsomega.4c07888
ACS Omega 2025, 10, 833−847

in solution, the reaction catalyzed by $AlCl_3$ and $GaCl_3$ occurs via a two-step mechanism involving the formation of two TSs and a stable intermediate, where each TS exhibits an asynchronous character for both the endo and exo pathways. Nevertheless, in polar solvents, the *endo*-BF_3 reaction diverges from this established pattern: it displays only one TS and there is no intermediate. Moreover, the DFT calculations have demonstrated that the LAs play additional roles, i.e., (i) it forms stable complexes with the O atom of the carbonyl group of acrolein, and (ii) $AlCl_3$ and $GaCl_3$ form dimers, which impact the different equilibria. The above conclusions have been drawn by considering acrolein in its most stable s-trans conformation. Nevertheless, as shown by additional DFT calculations, the s-cis conformer having an estimated Maxwell−Boltzmann population of 2%, presents similar thermodynamic and kinetic characteristics.

This paper has thus paved the way toward a better understanding of the reactivity of 2,5-DMF, a direct product of biomass transformation. Future studies by our group will address the Diels−Alder reaction using more sophisticated dienophiles and furan-based dienes such as 5-hydroxymethylfurfural and its oxidized derivatives.

■ ASSOCIATED CONTENT

Supporting Information

The Supporting Information is available free of charge at https://pubs.acs.org/doi/10.1021/acsomega.4c07888.

The chemical descriptors of the reactants (2,5-DMF, acrolein, and acrolein-LA) in solution (cyclohexane, dichloromethane, ethanol, and DMSO); the list of thermochemical data, reaction rate constants, the endo/exo ratio, and the geometries of the TSs for the uncatalyzed and LA-catalyzed DA reactions between 2,5-DMF **1** and acrolein **2** in the predicted solvents, thermochemical data of the LAs complexation reactions with solvent molecules and with the oxygen atom of acrolein, chemical descriptors of the activated alkenes **2a−2g**, as well as the geometries of the TSs of the uncatalyzed DA reactions between 2,5-DMF **1** and the activated alkenes **2a−2g** (PDF)

■ AUTHOR INFORMATION

Corresponding Author

Vincent Liégeois − *Laboratory of Theoretical Chemistry, Theoretical and Structural Physical Chemistry Unit, Namur Institute of Structured Matter (NISM), University of Namur, B-5000 Namur, Belgium;* orcid.org/0000-0003-2919-8025; Phone: + 32 81 724553; Email: vincent.liegeois@unamur.be

Authors

Mohamed Chellegui − *Laboratory of Organic Chemistry (LR17ES08), Faculty of Sciences, University of Sfax, 3038 Sfax, Tunisia; Laboratory of Theoretical Chemistry, Theoretical and Structural Physical Chemistry Unit, Namur Institute of Structured Matter (NISM), University of Namur, B-5000 Namur, Belgium*

Mahmoud Trabelsi − *Laboratory of Organic Chemistry (LR17ES08), Faculty of Sciences, University of Sfax, 3038 Sfax, Tunisia*

Benoît Champagne − *Laboratory of Theoretical Chemistry, Theoretical and Structural Physical Chemistry Unit, Namur Institute of Structured Matter (NISM), University of Namur, B-5000 Namur, Belgium;* orcid.org/0000-0003-3678-8875

Complete contact information is available at: https://pubs.acs.org/10.1021/acsomega.4c07888

Notes

The authors declare no competing financial interest.

■ ACKNOWLEDGMENTS

The authors are grateful to the ARES-CCD and the Ministry of Higher Education and Scientific Research of Tunisia, which financially supported this work. M.C. is also grateful to UNamur for financially contributing to his research stay. V.L. thanks the F.R.S.-FNRS for his Senior Research Associate position. The calculations were performed on the computers of the "Consortium des équipements de Calcul Intensif (CÉCI)" (http://www.ceci-hpc.be), including those of the "UNamur Technological Platform of High-Performance Computing (PTCI)" (http://www.ptci.unamur.be), for which we gratefully acknowledge the financial support from the FNRS-FRFC, the Walloon Region, and the University of Namur (Conventions nos. U.G006.15, U.G018.19, U.G011.22, RW1610468, RW/GEQ2016, RW2110213, and RW2210148).

■ REFERENCES

(1) Vispute, T. P.; Zhang, H.; Sanna, A.; Xiao, R.; Huber, G. W. Renewable Chemical Commodity Feedstocks from Integrated Catalytic Processing of Pyrolysis Oils. *Science* **2010**, *330*, 1222−1227.

(2) Carlson, T. R.; Tompsett, G. A.; Conner, W. C.; Huber, G. W. Aromatic Production from Catalytic Fast Pyrolysis of Biomass-Derived Feedstocks. *Top. Catal.* **2009**, *52*, 241−252.

(3) Cheng, Y.-T.; Jae, J.; Shi, J.; Fan, W.; Huber, G. W. Production of Renewable Aromatic Compounds by Catalytic Fast Pyrolysis of Lignocellulosic Biomass with Bifunctional Ga/ZSM-5 Catalysts. *Angew. Chem., Int. Ed.* **2012**, *51*, 1387−1390.

(4) Tomás, R. A.; Bordado, J. C.; Gomes, J. F. P-Xylene Oxidation to Terephthalic Acid: A Literature Review Oriented Toward Process Optimization and Development. *Chem. Rev.* **2013**, *113*, 7421−7469.

(5) Pacheco, J. J.; Labinger, J. A.; Sessions, A. L.; Davis, M. E. Route to Renewable PET: Reaction Pathways and Energetics of Diels−Alder and Dehydrative Aromatization Reactions between Ethylene and Biomass-Derived Furans Catalyzed by Lewis Acid Molecular Sieves. *ACS Catal.* **2015**, *5*, 5904−5913.

(6) Pacheco, J. J.; Davis, M. E. Synthesis of Terephthalic Acid via Diels-Alder Reactions with Ethylene and Oxidized Variants of 5-Hydroxymethylfurfural. *Proc. Natl. Acad. Sci. U.S.A.* **2014**, *111*, 8363−8367.

(7) Wantanachaisaeng, P.; O'Neil, K. *Capturing Opportunities for Para-Xylene Production*; UOP LLC, 2007.

(8) Moliner, M.; Román-Leshkov, Y.; Davis, M. E. Tin-containing Zeolites are Highly Active Catalysts for the Isomerization of Glucose in Water. *Proc. Natl. Acad. Sci. U.S.A.* **2010**, *107*, 6164−6168.

(9) Insyani, R.; Verma, D.; Kim, S. M.; Kim, J. Direct One-Pot Conversion of Monosaccharides into High-Yield 2,5-Dimethylfuran Over a Multifunctional Pd/Zr-Based Metal−Organic Framework@Sulfonated Graphene Oxide Catalyst. *Green Chem.* **2017**, *19*, 2482−2490.

(10) Gallezot, P. Conversion of Biomass to Selected Chemical Products. *Chem. Soc. Rev.* **2012**, *41*, 1538−1558.

(11) Van Putten, R. J.; Van Der Waal, J. C.; De Jong, E. D.; Rasrendra, C. B.; Heeres, H. J.; de Vries, J. G. Hydroxymethylfurfural, a Versatile Platform Chemical Made from Renewable Resources. *Chem. Rev.* **2013**, *113*, 1499−1597.

(12) Wang, T.; Nolte, M. W.; Shanks, B. H. Catalytic Dehydration of C 6 Carbohydrates for the Production of Hydroxymethylfurfural

(HMF) as a Versatile Platform Chemical. *Green Chem.* **2014**, *16*, 548−572.
(13) Nikolla, E.; Román-Leshkov, Y.; Moliner, M.; Davis, M. E. One-Pot" Synthesis of 5-(Hydroxymethyl) Furfural from Carbohydrates Using Tin-Beta Zeolite. *ACS Catal.* **2011**, *1*, 408−410.
(14) Reichert, J.; Brunner, B.; Jess, A.; Wasserscheid, P.; Albert, J. Biomass Oxidation to Formic Acid in Aqueous Media Using Polyoxometalate Catalysts−Boosting FA Selectivity by In-Situ Extraction. *Energy Environ. Sci.* **2015**, *8*, 2985−2990.
(15) Lewkowski, J. Synthesis Chemistry and Applications of 5-Hydroxymethylfurfural and its Derivatives. *Arkivoc* **2001**, *2001*, 17−54.
(16) Ståhlberg, T.; Fu, W.; Woodley, J. M.; Riisager, A. Synthesis of 5-(Hydroxymethyl) Furfural in Ionic Liquids: Paving the Way to Renewable Chemicals. *ChemSusChem* **2011**, *4*, 451−458.
(17) Ståhlberg, T.; Rodriguez-Rodriguez, S.; Fristrup, P.; Riisager, A. Metal-Free Dehydration of Glucose to 5-(Hydroxymethyl) Furfural in Ionic Liquids with Boric Acid as a Promoter. *Chem.—Eur. J.* **2011**, *17*, 1456−1464.
(18) James, O. O.; Maity, S.; Usman, L. A.; Ajanaku, K. O.; Ajani, O. O.; Siyanbola, T. O.; Sahu, S.; Chaubey, R. Towards the Conversion of Carbohydrate Biomass Feedstocks to Biofuels via Hydroxylmethylfurfural. *Energy Environ. Sci.* **2010**, *3*, 1833−1850.
(19) Rosatella, A. A.; Simeonov, S. P.; Frade, R. F.; Afonso, C. A. 5-Hydroxymethylfurfural (HMF) as a Building Block Platform: Biological Properties, Synthesis and Synthetic Applications. *Green Chem.* **2011**, *13*, 754−793.
(20) Bicker, M.; Hirth, J.; Vogel, H. Dehydration of Fructose to 5-Hydroxymethylfurfural in Sub-and Supercritical Acetone. *Green Chem.* **2003**, *5*, 280−284.
(21) Román-Leshkov, Y.; Barrett, C. J.; Liu, Z. Y.; Dumesic, J. A. Production of Dimethylfuran for Liquid Fuels from Biomass-Derived Carbohydrates. *Nature* **2007**, *447*, 982−985.
(22) Diels, O.; Alder, K. Synthesen in der hydro-aromatischen Reihe, II. Mitteilung: Über Cantharidin. *Ber. Dtsch. Chem. Ges.* **1929**, *62*, 554−562.
(23) Diels, O.; Alder, K. Synthesen in Der Hydroaromatischen Reihe, V. Mitteilung: Über Δ4-Tetrahydro-o-Phthalsäure Stellungnahme zu der Mitteilung von EH Farmer und FL Warren: Eigenschaften Konjugierter Doppelbindungen (VII). *Ber. Dtsch. Chem. Ges.* **1929**, *62*, 2087−2090.
(24) Nikbin, N.; Do, P. T.; Caratzoulas, S.; Lobo, R. F.; Dauenhauer, P. J.; Vlachos, D. G. A DFT Study of the Acid-Catalyzed Conversion of 2,5-Dimethylfuran and Ethylene to P-Xylene. *J. Catal.* **2013**, *297*, 35−43.
(25) Nikbin, N.; Feng, S.; Caratzoulas, S.; Vlachos, D. G. P-Xylene Formation by Dehydrative Aromatization of a Diels−Alder Product in Lewis and Brønsted Acidic Zeolites. *J. Phys. Chem. C* **2014**, *118*, 24415−24424.
(26) Rohling, R. Y.; Tranca, I. C.; Hensen, E. J.; Pidko, E. A. Electronic Structure Analysis of the Diels−Alder Cycloaddition Catalyzed by Alkali-Exchanged Faujasites. *J. Phys. Chem. C* **2018**, *122*, 14733−14743.
(27) Patet, R. E.; Fan, W.; Vlachos, D. G.; Caratzoulas, S. Tandem Diels−Alder Reaction of Dimethylfuran and Ethylene and Dehydration to Para-Xylene Catalyzed by Zeotypic Lewis Acids. *ChemCatChem* **2017**, *9*, 2523−2535.
(28) Chang, C. C.; Je Cho, H.; Yu, J.; Gorte, R. J.; Gulbinski, J.; Dauenhauer, P.; Fan, W. Lewis Acid Zeolites for Tandem Diels−Alder Cycloaddition and Dehydration of Biomass-Derived Dimethylfuran and Ethylene to Renewable P-Xylene. *Green Chem.* **2016**, *18*, 1368−1376.
(29) Chellegui, M.; Champagne, B.; Trabelsi, M. Lewis Acid-Catalyzed Diels−Alder Cycloaddition of 2,5-Dimethylfuran and Ethylene−A Density Functional Theory Investigation. *Theor. Chem. Acc.* **2022**, *141*, 21.
(30) Mahmoud, E.; Watson, D. A.; Lobo, R. F. Renewable Production of Phthalic Anhydride from Biomass-Derived Furan and Maleic Anhydride. *Green Chem.* **2014**, *16*, 167−175.
(31) Salavati-fard, T.; Caratzoulas, S.; Doren, D. J. DFT Study of Solvent Effects in Acid-Catalyzed Diels−Alder Cycloadditions of 2,5-Dimethylfuran and Maleic Anhydride. *J. Phys. Chem. A* **2015**, *119*, 9834−9843.
(32) Ju, Z.; Yao, X.; Liu, X.; Ni, L.; Xin, J.; Xiao, W. Theoretical Study on the Conversion Mechanism of Biobased 2,5-Dimethylfuran and Acrylic Acid into Aromatics Catalyzed by Brønsted Acid Ionic Liquids. *Ind. Eng. Chem. Res.* **2019**, *58*, 11111−11120.
(33) Ni, L.; Xin, J.; Dong, H.; Lu, X.; Liu, X.; Zhang, S. A Simple and Mild Approach for the Synthesis of p-Xylene from Bio-Based 2,5-Dimethyfuran by Using Metal Triflates. *ChemSusChem* **2017**, *10*, 2394−2401.
(34) Shiramizu, M.; Toste, F. D. On the Diels−Alder Approach to Solely Biomass-Derived Polyethylene Terephthalate (PET): Conversion of 2,5-Dimethylfuran and Acrolein into p-Xylene. *Chem.—Eur. J.* **2011**, *17*, 12452−12457.
(35) Fringuelli, F.; Piermatti, O.; Pizzo, F.; Vaccaro, L. Recent Advances in Lewis Acid Catalyzed Diels−Alder Reactions in Aqueous Media. *Eur. J. Org Chem.* **2001**, *2001*, 439−455.
(36) Yates, P.; Eaton, P. Acceleration of the Diels-Alder Reaction by Aluminum Chloride. *J. Am. Chem. Soc.* **1960**, *82*, 4436−4437.
(37) Fringuelli, F.; Taticchi, A.; Wenkert, E. Diels-Alder Reactions of Cycloalkenones in Organic Synthesis. *Org. Prep. Proced. Int.* **1990**, *22*, 131−165.
(38) Fringuelli, F.; Minuti, L.; Pizzo, F.; Taticchi, A.; Consiglio, G.; Chanon, M.; Striley, C.; Weidlein, J.; Nasiri, A.; Okada, Y. Reactivity and Selectivity in Lewis-Acid-Catalyzed Diels-Alder Reactions of 2-Cyclohexenones. *Acta Chem. Scand.* **1993**, *47*, 255−263.
(39) *Lewis Acid Reagents: a Practical Approach*; Yamamoto, H., Ed.; Oxford University Press, 1999;
(40) Lee, M. W.; Herndon, W. C. Stereochemistry of the Furan-Maleic Anhydride Cycloaddition. *J. Org. Chem.* **1978**, *43*, 518.
(41) Gonzalez, J.; Houk, K. N. Ab initio Transition Structures for Diels-Alder Reactions of 2-Azabutadiene with Alkenes and Alkynes: Effects of Substituents, the Aza Group, and Catalysis on Reactivity. *J. Org. Chem.* **1992**, *57*, 3031−3037.
(42) Domingo, L. R.; Picher, M. T.; José Aurell, M. A DFT Characterization of the Mechanism for the Cycloaddition Reaction between 2-Methylfuran and Acetylenedicarboxylic Acid. *J. Phys. Chem. A* **1999**, *103*, 11425−11430.
(43) Avalos, M.; Babiano, R.; Bravo, J. L.; Cintas, P.; Jiménez, J. L.; Palacios, J. C.; Silva, M. A. Computational Studies on the BF3-Catalyzed Cycloaddition of Furan with Methyl Vinyl Ketone: a New Look at Lewis Acid Catalysis. *J. Org. Chem.* **2000**, *65*, 6613−6619.
(44) Fraile, J. M.; García, J.; Gómez, M.; de la Hoz, A.; Mayoral, J. A.; Moreno, A.; Prieto, P.; Salvatella, L.; Vázquez, E. Tandem Diels−Alder Aromatization Reactions of Furans under Unconventional Reaction Conditions− Experimental and Theoretical Studies. *Eur. J. Org Chem.* **2001**, *2001*, 2891−2899.
(45) Domingo, L. R.; Asensio, A.; Arroyo, P. Density Functional Theory Study of the Lewis Acid-Catalyzed Diels−Alder Reaction of Nitroalkenes with Vinyl Ethers using Aluminum Derivatives. *J. Phys. Org. Chem.* **2002**, *15*, 660−666.
(46) Sáez, J. A.; Arnó, M.; Domingo, L. R. Lewis Acid-Catalyzed [4 + 3] Cycloaddition of 2-(Trimethyl Silyloxy) Acrolein with Furan. Insight on the Nature of the Mechanism from a DFT Analysis. *Org. Lett.* **2003**, *5*, 4117−4120.
(47) Alves, C. N.; Carneiro, A. S.; Andrés, J.; Domingo, L. R. A DFT study of the Diels−Alder Reaction between Methyl Acrolein Derivatives and Cyclopentadiene. Understanding the Effects of Lewis Acids Catalysts based on Sulfur Containing Boron Heterocycles. *Tetrahedron* **2006**, *62*, 5502−5509.
(48) Nacereddine, A. K.; Yahia, W.; Sobhi, C.; Djerourou, A. A Theoretical Study of the Mechanism and Stereoselectivity of the Diels−Alder Cycloaddition between Difluoro-2-MethylenCyclopropane and Furan. *Tetrahedron Lett.* **2012**, *53*, 5784−5786.
(49) Bouacha, S.; Nacereddine, A. K.; Djerourou, A. A Theoretical Study of the Mechanism, Stereoselectivity and Lewis Acid Catalyst on

https://doi.org/10.1021/acsomega.4c07888
ACS Omega 2025, 10, 833−847

the Diels−Alder Cycloaddition between Furan and Activated Alkenes. *Tetrahedron Lett.* **2013**, *54*, 4030−4033.
(50) Li, P.; Liu, F.; Shao, Y.; Mei, Y. Computational Insights into endo/exo Selectivity of the Diels−Alder Reaction in Explicit Solvent at Ab Initio Quantum Mechanical/Molecular Mechanical Level. *J. Phys. Chem. B* **2019**, *123*, 5131−5138.
(51) Sakata, K.; Fujimoto, H. Roles of Lewis Acid Catalysts in Diels-Alder Reactions between Cyclopentadiene and Methyl Acrylate. *ChemistryOpen* **2020**, *9*, 662−666.
(52) Lording, W. J.; Fallon, T.; Sherburn, M. S.; Paddon-Row, M. N. The Simplest Diels−Alder Reactions are not Endo-Selective. *Chem. Sci.* **2020**, *11*, 11915−11926.
(53) Fukui, K. Role of Frontier Orbitals in Chemical Reactions. *Science* **1982**, *218*, 747−754.
(54) Moore, J. A.; Partain, E. M., III Catalyzed Addition of Furan with Acrylic Monomers. *J. Org. Chem.* **1983**, *48*, 1105−1106.
(55) Khan, T. S.; Gupta, S.; Ahmad, M.; Alam, M. I.; Haider, M. A. Effect of Substituents and Promoters on the Diels−Alder Cycloaddition Reaction in the Biorenewable Synthesis of Trimellitic Acid. *RSC Adv.* **2020**, *10*, 30656−30670.
(56) Domingo, L. R.; Arnó, M.; Andres, J. Influence of Reactant Polarity on the Course of the Inverse-Electron-Demand Diels−Alder Reaction. A DFT Study of Regio-and Stereoselectivity, Presence of Lewis Acid Catalyst, and Inclusion of Solvent Effects in the Reaction between Nitroethene and Substituted Ethenes. *J. Org. Chem.* **1999**, *64*, 5867−5875.
(57) Domingo, L. R.; Sáez, J. A. Understanding the Mechanism of Polar Diels−Alder Reactions. *Org. Biomol. Chem.* **2009**, *7*, 3576−3583.
(58) Domingo, L. R. A New C−C Bond Formation Model Based on the Quantum Chemical Topology of Electron Density. *RSC Adv.* **2014**, *4*, 32415−32428.
(59) Domingo, L. R.; Ríos-Gutiérrez, M.; Silvi, B.; Pérez, P. The Mysticism of Pericyclic Reactions: a Contemporary Rationalisation of Organic Reactivity based on Electron Density Analysis. *Eur. J. Org Chem.* **2018**, *2018*, 1107−1120.
(60) Domingo, L. R.; Ríos-Gutiérrez, M.; Pérez, P. Unveiling the Lewis Acid Catalyzed Diels−Alder Reactions Through the Molecular Electron Density Theory. *Molecules* **2020**, *25*, 2535−2560.
(61) Fernández, I.; Bickelhaupt, F. M. Deeper Insight into the Diels−Alder Reaction Through the Activation Strain Model. *Chem.—Asian J.* **2016**, *11*, 3297−3304.
(62) Vermeeren, P.; Hamlin, T. A.; Fernández, I.; Bickelhaupt, F. M. How Lewis Acids Catalyze Diels-Alder Reactions. *Angew. Chem., Int. Ed.* **2020**, *59*, 6201−6206.
(63) Zhao, Y.; Truhlar, D. G. The M06 Suite of Density Functionals for Main Group Thermochemistry, Thermochemical Kinetics, Noncovalent Interactions, Excited States, and Transition Elements: Two New Functionals and Systematic Testing of Four M06-Class Functionals and 12 other Functionals. *Theor. Chem. Acc.* **2008**, *120*, 215−241.
(64) Fukui, K. The Path of Chemical Reactions-the IRC Approach. *Acc. Chem. Res.* **1981**, *14*, 363−368.
(65) Tomasi, J.; Mennucci, B.; Cammi, R. Quantum Mechanical Continuum Solvation Models. *Chem. Rev.* **2005**, *105*, 2999−3094.
(66) Kelly, C. P.; Cramer, C. J.; Truhlar, D. G. SM6: A Density Functional Theory Continuum Solvation Model for Calculating Aqueous Solvation Free Energies of Neutrals, Ions, and Solute−Water Clusters. *J. Chem. Theory Comput.* **2005**, *1*, 1133−1152.
(67) Wynne-Jones, W. F.; Eyring, H. The Absolute Rate of Reactions in Condensed Phases. *J. Chem. Phys.* **1935**, *3*, 492−502.
(68) Reed, A. E.; Curtiss, L. A.; Weinhold, F. Intermolecular Interactions from a Natural Bond Orbital, Donor-Acceptor Viewpoint. *Chem. Rev.* **1988**, *88*, 899−926.
(69) Krokidis, X.; Noury, S.; Silvi, B. Characterization of Elementary Chemical Processes by Catastrophe Theory. *J. Phys. Chem. A* **1997**, *101*, 7277−7282.
(70) Becke, A. D.; Edgecombe, K. E. A Simple Measure of Electron Localization in Atomic and Molecular Systems. *J. Chem. Phys.* **1990**, *92*, 5397−5403.
(71) Silvi, B.; Savin, A. Classification of Chemical Bonds Based on Topological Analysis of Electron Localization Functions. *Nature* **1994**, *371*, 683−686.
(72) Noury, S.; Krokidis, X.; Fuster, F.; Silvi, B. Computational Tools for the Electron Localization Function Topological Analysis. *Comput. Chem.* **1999**, *23*, 597−604.
(73) Liégeois, V. DrawMol; UNamur, www.unamur.be/drawmol (accessed September 1, 2024), 2024.
(74) Liégeois, V. DrawProfile; UNamur, www.unamur.be/drawprofile (accessed September 1, 2024), 2024.
(75) Parr, R. G.; Yang, W. *Density Functional Theory of Atoms and Molecules*; Oxford University Press: New York, 1989.
(76) Geerlings, P.; De Proft, F.; Langenaeker, W. Conceptual Density Functional Theory. *Chem. Rev.* **2003**, *103*, 1793−1874.
(77) Domingo, L. R.; Ríos-Gutiérrez, M.; Pérez, P. Applications of the Conceptual Density Functional Theory Indices to Organic Chemistry Reactivity. *Molecules* **2016**, *21*, 748−769.
(78) Parr, R. G.; Szentpály, L. V.; Liu, S. Electrophilicity Index. *J. Am. Chem. Soc.* **1999**, *121*, 1922−1924.
(79) Parr, R. G.; Pearson, R. G. Absolute Hardness: Companion Parameter to Absolute Electronegativity. *J. Am. Chem. Soc.* **1983**, *105*, 7512−7516.
(80) Domingo, L. R.; Chamorro, E.; Pérez, P. Understanding the Reactivity of Captodative Ethylenes in Polar Cycloaddition Reactions. A Theoretical Study. *J. Org. Chem.* **2008**, *73*, 4615−4624.
(81) Domingo, L. R.; Aurell, M. J.; Pérez, P.; Contreras, R. Quantitative Characterization of the Global Electrophilicity Power of Common Diene/Dienophile Pairs in Diels−Alder Reactions. *Tetrahedron* **2002**, *58*, 4417−4423.
(82) van Zeist, W. J.; Bickelhaupt, F. M. The Activation Strain Model of Chemical Reactivity. *Org. Biomol. Chem.* **2010**, *8*, 3118−3127.
(83) Fernández, I.; Bickelhaupt, F. M. The Activation Strain Model and Molecular Orbital Theory: Understanding and Designing Chemical Reactions. *Chem. Soc. Rev.* **2014**, *43*, 4953−4967.
(84) Bickelhaupt, F. M.; Houk, K. N. Analyzing Reaction Rates with the Distortion/Interaction-Activation Strain Model. *Angew. Chem., Int. Ed. Engl.* **2017**, *56*, 10070−10086.
(85) Svatunek, D.; Houk, K. N. AutoDIAS: A Python Tool for an Automated Distortion/Interaction Activation Strain Analysis. *J. Comput. Chem.* **2019**, *40*, 2509−2515.
(86) Frisch, M. J.; Trucks, G. W.; Schlegel, H. B.; Scuseria, G. E.; Robb, M. A.; Cheeseman, J. R.; Scalmani, G.; Barone, V.; Mennucci, B.; Petersson, G. A.; Nakatsuji, H.; Caricato, M.; Li, X.; Hratchian, H. P.; Izmaylov, A. F.; Bloino, J.; Zheng, G.; Sonnenberg, J. L.; Hada, M.; Ehara, M.; Toyota, K.; Fukuda, R.; Hasegawa, J.; Ishida, M.; Nakajima, T.; Honda, Y.; Kitao, O.; Nakai, H.; Vreven, T.; Montgomery, J. A., Jr.; Peralta, J. E.; Ogliaro, F.; Bearpark, M.; Heyd, J. J.; Brothers, E.; Kudin, K. N.; Staroverov, V. N.; Kobayashi, R.; Normand, J.; Raghavachari, K.; Rendell, A.; Burant, J. C.; Iyengar, S. S.; Tomasi, J.; Cossi, M.; Rega, N.; Millam, J. M.; Klene, M.; Knox, J. E.; Cross, J. B.; Bakken, V.; Adamo, C.; Jaramillo, J.; Gomperts, R.; Stratmann, R. E.; Yazyev, O.; Austin, A. J.; Cammi, R.; Pomelli, C.; Ochterski, J. W.; Martin, R. L.; Morokuma, K.; Zakrzewski, V. G.; Voth, G. A.; Salvador, P.; Dannenberg, J. J.; Dapprich, S.; Daniels, A. D.; Farkas, O.; Foresman, J. B.; Ortiz, J. V.; Cioslowski, J.; Fox, D. J. *Gaussian 16*. Revision A.01; Gaussian, Inc.: Wallingford, CT, 2016.
(87) Jaramillo, P.; Domingo, L. R.; Chamorro, E.; Pérez, P. A Further Exploration of a Nucleophilicity Index Based on the Gas-Phase Ionization Potentials. *J. Mol. Struct.:THEOCHEM* **2008**, *865*, 68−72.
(88) Domingo, L. R.; Arnó, M.; Sáez, J. A. DFT study of the molecular mechanism of Lewis acid induced [4 + 3] cycloadditions of 2-alkylacroleins with cyclopentadiene. *J. Org. Chem.* **2009**, *74*, 5934−5940.

https://doi.org/10.1021/acsomega.4c07888
ACS Omega 2025, 10, 833−847

(89) Fernández, I.; Bickelhaupt, F. M. Origin of the "Endo Rule" in Diels−Alder Reactions. *J. Comput. Chem.* **2014**, *35*, 371−376.
(90) Fernández, I. Combined Activation Strain Model and Energy Decomposition Analysis Methods: A New Way to Understand Pericyclic Reactions. *Phys. Chem. Chem. Phys.* **2014**, *16*, 7662−7671.
(91) Mahaut, D.; Chardon, A.; Mineur, L.; Berionni, G.; Champagne, B. Rational Development of a Metal-Free Bifunctional System for the C−H Activation of Methane: A Density Functional Theory Investigation. *ChemPhysChem* **2021**, *22*, 1958−1966.

https://doi.org/10.1021/acsomega.4c07888
ACS Omega 2025, 10, 833−847